Okinawa Institute of Science and Technology
Graduate University

Thesis submitted for the degree

Doctor of Philosophy

Functional roles of microtubules in a giant presynaptic terminal

by

Lashmi Piriya Ananda Babu

Supervisor: Professor. Tomoyuki Takahashi
Co-Supervisor: Professor. Jeffery Wickens

February, 2018

Declaration of Original and Sole Authorship

I, Lashmi Piriya Ananda Babu, declare that this thesis entitled functional roles of microtubules in a giant presynaptic terminal and the data presented in it are original and my own work.

I confirm that:

No part of this work has previously been submitted for a degree at this or any other university.

References to the work of others have been clearly acknowledged. Quotations from the work of others have been clearly indicated, and attributed to them.

In cases where others have contributed to part of this work, such contribution has been clearly acknowledged and distinguished from my own work.

Date: February, 2018

Declaration of Original and Sole Authorship

Signature:

Acknowledgements

First and foremost, I would like to thank my supervisor Dr. Tomoyuki Takahashi for giving me the opportunity to conduct my Ph.D. studies in his group, for being a role model scientist of both tremendous skill and knowledge and for always guiding me to narrow down my focus every time I got distracted in science. I believe the lessons I learned with him are for life.

I am grateful to the members of my Ph.D. committee, Dr. Jeffery Wickens and Dr. Bernd Kuhn for their ongoing support throughout my Ph.D. years.

I would like to thank all members of Cellular and Molecular Synaptic Function Unit for their assistance, discussions, friendships and a great working atmosphere that made every minute of work worth the while. Dr. Laurent Guillaud and Dr. Kohgaku Eguchi deserve a special ‘thanks’ for training me in imaging and electrophysiology, respectively. I am extremely grateful to Dr. Tetsuya Hori for teaching and boosting my confidence in performing pair recording, and for always being available for in-depth scientific discussions. I am also extremely grateful to Dr. Yukihiro Nakamura for teaching deconvolution analysis and for his valuable inputs. I would like to thank Dr. Toshio Sasaki for excellent technical assistance in performing EM. Special thanks go to Dr. Yasushi Okada for allowing us to use his STED microscope set up at RIKEN-qBIC used in this study.

I would like to express my gratitude to the faculty members of the OIST Ph.D. program for giving me the opportunity to study in this exciting field and within the wonderful scientific community in Okinawa. Additionally, I would like to thank all the members of Graduate School and student support section for making my life lot easier through their incessant support and care throughout these years.

Last but not least, I would like to thank my parents and my friends within and outside OIST for all the love and support they gave me throughout my student years.

Abstract

The functional roles of cytoskeletal elements actin and microtubule are well established in various cellular processes. However, their role in axon terminals is still unclear. Here, I started my thesis study by questioning the role of actin filaments at the calyx of Held presynaptic terminals in developing rats before and after hearing onset. Having observed that actin filaments are involved in synaptic vesicle recruitment in pre-hearing rats, but not in post-hearing rats, I then proceeded to address the functional roles of the other cytoskeletal element, namely microtubules in rats after hearing onset. I have used a combination of tools to address both the functional and morphological aspects. I found that both cytoskeletal elements play significant roles in regulating synaptic transmission.

CONTENTS

1. BACKGROUND

1.1 Neuronal communications

Brain functions rely on the ability of neurons to communicate through contacts between them. Communications between neurons occur at cell-cell contact sites called synapses (Sherrington, 1906). In chemical synapses, electrical information is transferred by the release of neurotransmitter from presynaptic neurons, followed by a detection of neurotransmitter signals by postsynaptic neurons. At a chemical synapse, the arrival of an action potential (AP) at a presynaptic terminal activates voltage-gated Ca^{2+} channels (VGCCs), thereby inducing a rapid influx of Ca^{2+} (Katz and Miledi, 1969). Recent studies have revealed that VGCCs are present as clusters of variable sizes at the active zone (AZ) (Holderith et al., 2012; Nakamura et al., 2015). This rapid influx of Ca^{2+} ions is sensed by a protein on synaptic vesicles (SVs) called synaptotagmins. Synaptotagmin-1, -2 and -5/9 mediate fast synchronous transmitter release (Xu et al., 2007; Kerr et al., 2008), whereas synaptotagmin-7 mediates slow asynchronous release (Luo and Sudhof, 2017). Binding of Ca^{2+} to the C_2 domains of the synaptotagmins (-1, -2, -5/9) triggers exocytosis of SVs, pre-docked to release sites mediated by SNARE (soluble NSF attachment protein receptors) complex (Pang et al., 2006). This release process is highly stochastic, as in most terminals APs trigger neurotransmitter release at a fraction of release sites. Neurotransmitters are released into the synaptic cleft and bind to postsynaptic receptors. There are two types of receptors; ionotropic receptors (ligand-gated ion channels) and metabotropic receptors (G protein-coupled receptors) of which the former mediates fast neurotransmission. Postsynaptic receptors induce changes in membrane potential, membrane conductance, and can eventually change gene expression.

1.2 Synaptic vesicle cycle

Sustained rapid information transfer in the nervous system relies on recycling of SVs, which undergo endocytosis, transmitter refilling, transport to release sites and reuse for exocytic transmitter release in presynaptic terminals. Schematic illustration of SV cycle is presented below (Illustration 1).

1.2.1 Priming of synaptic vesicles

According to a current view, SVs become release competent, by moving and docking to release sites in AZ of presynaptic terminal. AZs are electron-dense structures composed of evolutionarily conserved proteins, such as RIM, Munc13, RIM-BP, α-liprin, and ELKS, which are required for SV docking. The docked vesicles become release-competent (molecular priming) by interacting with SNAREs (see below) and Sec1/Munc18-like protein. After docking, SVs are thought to be re-localized closer to VGCC clusters (positional priming). The coupling distance between the Ca^{2+} sensor on SVs and VGCC cluster perimeter is estimated as 10- 30 nm at the calyx of Held synapse of rodents at P7-14 (Nakamura et al., 2015). Such a nanodomain ensures high Ca^{2+} concentration required for low-affinity Ca^{2+} sensor proteins, such as synaptotagmins, enabling rapid fusion of SVs. Recent studies suggest an involvement of actin filaments in positional priming of SVs (Lee et al., 2012a).

1.2.2 Exocytosis

The exocytosis of SVs occurs within a millisecond after the arrival of an AP at a nerve terminal. Fusion of vesicles with the plasma membrane (PM) is mediated by SNARE complex. This complex is composed of presynaptic PM proteins, syntaxin-1a (Qa SNARE) and SNAP-25 (t-SNARE, containing Qb and Qc SNARE motifs), and of the vesicular protein synaptobrevin (VAMP2, v-SNARE) (Sollner et al., 1993; Rizo and Rosenmund, 2008; Sudhof and Rothman, 2009). The SNARE proteins are characterized by 60-70 amino acid SNARE motifs. Before fusion, four SNARE protein motifs assemble into a four-helix coiled-coil structure, with one SNARE motif comprising synaptobrevin and syntaxin-1 and SNAP-25 forming a *trans*-SNARE (t-SNARE) complex. SVs are held in a release ready state where the t-SNARE complex is held in a partially zippered state. Ca^{2+} binding to synaptotagmin upon AP arrival causes the SNARE complex to fully zipper into tight conformation. In addition to synaptotagmin, complexin binds to Ca^{2+}, thereby competing with synaptotagmin for binding to SNARE complex (Melia, 2007). Another class of proteins called SM (Sec1/Munc-18) family binds directly to

syntaxin and SNAP-25 that serves as an acceptor for vesicle-bound synaptobrevin (Zilly et al., 2006). This complex formation ensures SVs to fuse into PM for the exocytic release of neurotransmitters.

1.2.3 Endocytosis

To maintain high-frequency transmission without completely exhausting SV pool, nerve terminals adopt highly efficient mechanisms to retrieve and re-use components of SV membrane from presynaptic PM in a process called endocytosis. An early study at frog neuromuscular junction (NMJ) revealed retrieval of vesicles after stimulation with little change in presynaptic structure (Ceccarelli et al., 1973), whereas another study demonstrated large endosome-like structures appearing inside the terminals after prolonged stimulation, from which new SVs bud off (Heuser and Reese, 1973). These pioneering studies established the classical concept of SV recycling in the nerve terminal. Subsequent studies revealed various recycling, including fusion-pore flicker called *kiss-and-run* (Ceccarelli et al., 1979). Two types of endocytosis, clathrin-mediated (CME) or clathrin-independent (CIE) endocytosis, are documented, of which, the former is generally thought to be the dominant form of recycling at most synapses. Upon strong stimulation, presynaptic PM area increases but quickly recovers by bulk endocytosis. Various endocytic adaptors and accessory proteins have been identified to orchestrate different stages of SVs formation from PM. These include clathrin, AP2, AP180, epsin, synaptotagmin, stonin, all of which are involved in recruiting and stabilizing clathrin. Thereafter, clathrin, epsin, endophilin, amphiphysin are recruited for clathrin lattice formation, and amphiphysin, dynamin play roles in fission of vesicles. Finally, Hsc70 and auxilin uncoat and reform fusion-competent vesicles (McMahon and Boucrot, 2011).

Recently, a new form of CIE called ultrafast endocytosis has been reported at mouse hippocampal synapses in culture using optogenetic stimulation followed by "flash-and-freeze" EM studies (Watanabe et al., 2013). Ultrafast endocytosis occurs within 50 -100 ms after exocytosis evoked by a 10-ms blue light pulse. It is proposed that actin filaments initialize membrane curvature to form large vesicles from presynaptic PM, which were eventually pinched off by dynamin. It is further

postulated that clathrin-coated vesicles bud from endosome-like vacuolar intermediates (Kononenko et al., 2014). Another study, using presynaptic capacitance measurements (C_m) reported that ultrafast endocytosis can occur at hippocampal and cerebellar mossy fiber terminals in slices at physiological temperature (PT) and likely involves actin and dynamin (Delvendahl et al., 2016). However, it is unknown whether ultrafast endocytosis or *kiss-and-run* contributes to fast reuse of SVs. Considering that the refilling time constant of glutamate into SVs is relatively slow (15 s at RT and 7 s at PT;(Hori and Takahashi, 2012)), the main role of rapid endocytosis might be just to maintain the terminal membrane structure deformed by massive vesicular fusion.

1.2.4 Re-acidification and refill of neurotransmitters

The endocytosed SVs are rapidly refilled with high concentrations of neurotransmitters *via* active transport driven by vacuolar proton pumps. The vacuolar-type H^+ ATPase establishes an electrochemical gradient ($\Delta\mu H^+$) across the vesicle membrane by exchanging luminal H^+ for cytosolic transmitters (Maycox et al., 1988a). It is a large multi-subunit protein complex extending from SVs with a large peripheral domain called V_1 for ATPase activity and an integral membrane domain called V_0 to mediate proton translocation. Although H^+ ATPase resembles F0/F1-ATPase found in mitochondria and bacteria; it functions by hydrolyzing ATP rather than generating ATP.

In case of the excitatory neurotransmitter glutamate, it is transported into SVs by vesicular glutamate transporters (VGLUT 1-3). VGLUT1 is predominantly found in neocortex and cerebellar cortex, whereas VGLUT2 is found mostly in brainstem nuclei, thalamic nuclei, cerebellar deep nuclei. Both VGLUT1 and VGLUT2 are co-expressed at some synapses such as those from hippocampal CA1 to CA3 neurons (Danik et al., 2005) or at the calyx of Held (Billups, 2005). VGLUT3 is transiently expressed in GABAergic, serotonergic, dopaminergic and cholinergic neurons in certain brain regions but not in glutamatergic neurons (Gras et al., 2005).

VGLUT1 deficient mice show impaired long-term potentiation (Balschun et al., 2010) and deletion of VGLUT2 in autaptic cultures of thalamic neurons results in a reduction in transmitter release (Moechars et al., 2006). VGLUT3 is the only isoform expressed in inner hair cell (IHC) and mice lacking VGLUT3 are entirely deaf due to the lack of glutamate release from IHC to the auditory nerve. VGLUT3 deficient mice also exhibit epilepsy (Seal and Edwards, 2006), anxiety-associated behaviors associated with reduced serotonergic transmission in dorsal raphe nuclei (Amilhon et al., 2010).

At the calyx of Held presynaptic terminal, where VGLUT1 and VGLUT2 colocalize (Billups, 2005), the time constant of glutamate refilling into SVs is determined, using caged glutamate photolysis, to be 15s at RT and 7 s at PT (Hori and Takahashi, 2012). This refilling rate is much faster than that previously determined in isolated vesicles (Maycox et al., 1988b; Carlson et al., 1989; Wolosker et al., 1996; Gras et al., 2002; Wilson et al., 2005) but much slower than the rate of rapid endocytosis. More recently, the refilling rate of GABA into SVs has been determined in cerebellar inhibitory neuronal pairs using caged GABA (Yamashita et al., 2018). The time constant of GABA refilling is estimated as 80s at RT and 40s at PT, and the time constant of recovery from activity-dependent depression was found to coincide with that of vesicular GABA uptake, suggesting that vesicular GABA refilling time can be a rate-limiting step for the recovery of IPSCs from synaptic depression.

1.2.5 Trafficking of synaptic vesicles

SVs, after retrieved from the terminal membrane or after budding off from endosomes, must be refilled with neurotransmitter and transported to release sites to be reused for release. However, such an SV trafficking has never been demonstrated. A 3D model simulation of vesicle movements suggests that hydrodynamic interactions and vesicle collisions might be the major determinants of vesicle mobility within the crowded presynaptic terminals (Rothman et al., 2016), whereas many directional SV movements are observed in resting calyceal and hippocampal nerve terminals (Guillaud et al., 2017). Nevertheless, stimulation-induced directional movements of SVs remain to be demonstrated in nerve terminals.

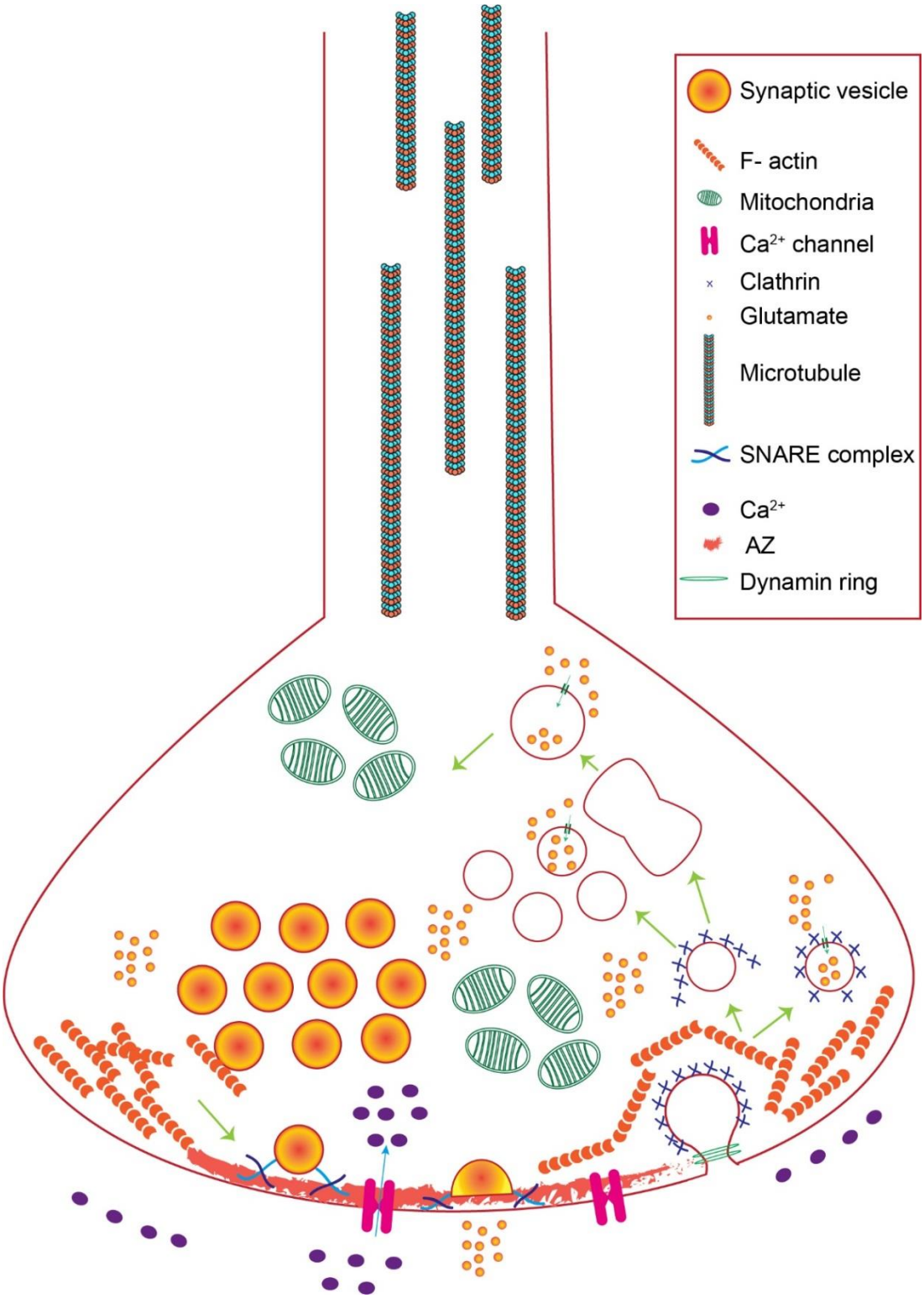

Illustration 1: Schematic illustration of SV cycles

Before exocytosis, SVs are docked and primed at the AZ. Following, Ca^{2+} influx through VGCCs, SVs undergoes exocytosis and release neurotransmitters into synaptic cleft. Endocytosis of SV membranes is thought to occur in peri-AZ and is predominantly mediated by clathrin dependent pathway. Newly endocytosed vesicles are refilled with transmitter using V-ATPase and reused for next round of exocytosis.

1.3 Synaptic vesicle pools

Presynaptic efficacy of synaptic transmission is determined by the number of vesicles released upon arrival of an AP and transmitter contents in individual SVs. SVs are conventionally divided into three pools: readily releasable pool (RRP), recycling pool, and reserve pool (Rizzoli and Betz, 2005). The vesicles in the RRP are thought to be docked at presynaptic AZ and primed for the release of neurotransmitter upon stimulation. At the calyx of Held, the RRP is divided into fast and slow releasing vesicle pools based on the release kinetics (Wu and Borst, 1999; Sakaba and Neher, 2001a). The observed difference in release kinetics could be attributed to the relative location of VGCCs to primed vesicles, where the vesicles closely positioned to the site of Ca^{2+} entry constitute the fast releasing pool (Wadel et al., 2007). Recycling pool consists of vesicles that release transmitter upon moderate stimulation and is estimated to comprise 5-20% of all vesicles (de Lange et al., 2003). Reserve pool includes vesicles that are recruited for release only upon intense stimulation after depletion of recycling pool and makes up for 80-90% of all vesicles. However, since this classification is based on results from experiments that utilized strong stimulation, the distinction between recycling pool and reserve pool is less obvious under physiological stimulation. Also, in a recent study at the calyx of Held of P7-9 rodents at room temperature (RT), the recycling pool is estimated to contain 200,000 vesicles (approx. 80% of total vesicles) and all of them are mobilized during repetitive firing (Qiu et al., 2015).

In addition to these pools, various kind of SV pools are postulated, which include a spontaneously releasing vesicle pool (Sara et al., 2005), “super-pool” implying pool of SVs traveling beyond single synaptic boutons (Darcy et al., 2006).

1.4 The calyx of Held

All the studies in the current thesis utilized the calyx of Held as the model synapse. The calyx of Held was first described in the auditory brainstem of cats in 1893 by the German anatomist Hans von Held using Golgi staining technique. The location, morphology, and properties of calyx provide an ideal system for studying synaptic transmission as summarized below. It is a giant axo-somatic glutamatergic nerve terminal that forms a part of the relay pathway involved in sound localization in the auditory brainstem. The calyx is a terminal of axonal fibers originating from globular bushy cells (GBCs) in the anterior ventral cochlear nucleus (aVCN), which crosses the midline and projects onto the principal neurons of the contralateral medial nucleus of the trapezoid body (MNTB). The calyx drives the principal neurons to provide both well-timed and sustained glycinergic inhibition to neurons in the superior olivary nucleus and many other brainstem nuclei. Apart from the calyceal input that generates fast-rising large EPSCs, the principal neurons also receive non-calyceal excitatory inputs that generate slow-rising small EPSCs (Hamann et al., 2003) and glycinergic inhibitory input from ventral nucleus of the trapezoid body (VNTB) (Albrecht et al., 2014). Also, a single GBC axon can form multiple calyces on different principal neurons (Kuwabara et al., 1991).

The characteristic features of the calyx that drives the principal neurons to high frequencies include large number of release sites, usually between 300-700 that are morphologically similar to other smaller conventional synapses (Satzler et al., 2002; Taschenberger et al., 2002), a large RRP ~ 2500 vesicles (Sakaba and Neher, 2001b), fast presynaptic calcium clearance, little delayed release and fast gating by glutamate receptor subunit 4 flop splice variant (GluR4) (Geiger et al., 1995; Koike-Tani et al., 2005). The AZs in the calyx have an average surface area of 0.1 μm^2 and positioned ~ 0.6 μm from each other (Satzler et al., 2002; Taschenberger et al., 2002). The pre-hearing rat calyx (P7-P10) expresses a mixture of calcium channel subtypes which includes N-, R-, and P/Q- type (Wu et al., 1998; Wu et al., 1999), however during development they switch to just P/Q- type calcium channels (Iwasaki and Takahashi, 1998; Iwasaki et al., 2000). The developmental switch of

VGCC subtypes is activity-dependent and involves BDNF and TrkB (Miki et al., 2013).

1.5 Involvement of presynaptic actin filaments in synaptic transmission

Globular actin (G-actin) is a ~ 42 kDa protein, abundantly expressed in presynaptic terminals, constituting ~ 2 % of synaptosomal proteins. The copy number of G-actin is ~22000 per presynaptic terminal, as estimated from immunoblotting and immunofluorescence analyses of cerebral cortical synaptosomes (Wilhelm et al., 2014). Actin filaments (F-actin) are composed of G-actin monomers assembled into double-stranded helix and held together by weak noncovalent interactions. This allows F-actin to assemble and disassemble dynamically, thereby restructuring the cytoskeleton. Actin is polymerized at barbed (+) end but depolymerized more slowly at pointed (-) end. This leads to net elongation of actin filaments at the barbed end (*actin treadmilling*). The energy for actin *treadmilling* is derived from hydrolysis of Mg^{2+} bound ATP in G-actin. This phenomenon of *treadmilling* is important to maintain dynamic cytoskeleton, which is also supported by actin-binding proteins, for shaping and remodeling the cytoarchitecture of the cell.

Various roles of actin are documented in the postsynaptic compartment, where actin is involved in anchoring and trafficking of AMPA (α-amino-3-hydroxy-5-methyl-4-isoxazole propionic acid) receptors and NMDA (*N*-methyl-D-aspartate) receptors at excitatory synapses (Allison et al., 1998) and scaffolding protein gephyrin at inhibitory synapses (Kirsch and Betz, 1995). Actin is also involved in activity-dependent remodeling of dendritic spine morphology (Fukazawa et al., 2003; Okamoto et al., 2004; Lin et al., 2005), which underlies long-term synaptic plasticity (Kim and Lisman, 1999; Krucker et al., 2000).

Early ultrastructural studies using quick freeze-etched EM revealed that at the presynaptic terminal SVs cluster, being interconnected to the meshwork of cytoskeletal filaments composed of actin and vesicle-associated phosphoprotein

synapsin (Landis et al., 1988; Hirokawa et al., 1989). Synapsin I binds to phospholipids on vesicle surface and can simultaneously interact with actin filaments via two high-affinity interaction sites (Greengard et al., 1994). Upon phosphorylation by CaM kinase II, synapsin I is detached from SVs as well as from cytoskeletal structures, thereby proposedly facilitate neurotransmitter release at the squid giant synapse (Llinas et al., 1991). At the frog NMJ, using actin-specific fluorescent probes, F-actin was found organized in a ladder-like pattern, co-localizing with β-fodrin, away from release sites (Dunaevsky and Connor, 2000), without co-localizing with SV clusters (Dunaevsky and Connor, 2000; Richards et al., 2004). Ultrastructural studies of lamprey reticulospinal giant synapses revealed that F-actin forms thin cytomatrix around SV clusters adjacent to the presynaptic plasma membrane and tethers vesicles (Shupliakov et al., 2002). Also, during stimulation F-actin colocalizes with synapsins at recycling or endocytic sites (Bloom et al., 2003). In cultured hippocampal neurons, green fluorescent protein (EGFP)-tagged actin forms a donut-shaped structure surrounding SV clusters (Morales et al., 2000), with 30% and 50 % of actin polymerized at rest and during stimulation, respectively (Sankaranarayanan et al., 2003). At cultured calyx-like presynaptic terminals, actin tagged with silicon-rhodamine (SiR-actin) was detected within the swellings at the distal end of the terminal (Guillaud et al., 2017), as previously demonstrated using phalloidin staining at the calyx of Held (Saitoh et al., 2001).

F-actin localized at the periphery of presynaptic terminals, in the vicinity of AZ may anchor SVs to form clusters in the pool of readily releasable SVs (Landis et al., 1988; Hirokawa et al., 1989; Dunaevsky and Connor, 2000; Shupliakov et al., 2002; Bloom et al., 2003; Sankaranarayanan et al., 2003; Richards et al., 2004). However, actin depolymerization with latrunculin A has no effect on SV clusters at cultured hippocampal synapses (Sankaranarayanan et al., 2003) or at frog NMJ (Richards et al., 2004). In contrast, at the *Drosophila* NMJ, actin depolymerization with cytochalasin D reportedly depletes SVs in RP (Kuromi and Kidokoro, 1998).

Apart from its role as a SV scaffold, actin might be involved in delivering SVs to AZ. At immature rodent calyx of Held presynaptic terminals, actin depolymerizer latrunculin A causes a significant delay in vesicle recruitment for recovery from synaptic depression, whereas actin stabilizer phalloidin reverses this effect of latrunculin A (Sakaba and Neher, 2003). Similar results are reported at snake NMJ (Cole et al., 2000). In contrast, in cultured hippocampal neurons, latrunculin A has no effect on the rate of RRP refilling (Morales et al., 2000). Latrunculin A blocks inter-bouton SV transport in hippocampal neurons in culture (Darcy et al., 2006).

The role of actin filaments in neurotransmitter release is controversial. Actin depolymerizing drugs increases mEPSC frequency at hippocampal synapses in culture (Morales et al., 2000) and in the slice (Meng et al., 2002). They also increase evoked EPSC amplitude (Morales et al., 2000) and rate of exocytosis measured by FM1-43 dye destaining (Sankaranarayanan et al., 2003). In contrast to these reports, F-actin is hypothesized to play roles in 'positional priming' of SVs at the release sites (Lee et al., 2012a).

Apart from being an integral part of cell cortex and an abundant force-generating molecule, actin has also been implicated to provide essential driving force for endocytosis in yeast (Engqvist-Goldstein and Drubin, 2003). In ultrastructural studies of lamprey reticulospinal giant synapses, F-actin is involved in SV endocytosis and transport of recycled vesicles to SV cluster (Shupliakov et al., 2002; Bloom et al., 2003). However, in the same preparation, latrunculin A has no effect on endocytosis, whereas phalloidin inhibits both exocytosis and endocytosis detected using FM1-43 (Bleckert et al., 2012). Likewise, actin depolymerizer cytochalasin D has no effect on FM1-43 uptake or release at the frog NMJ (Betz and Henkel, 1994), whereas, latrunculin A reduces both exocytosis and endocytosis monitored using FM1-43 (Richards et al., 2004). At hippocampal synapses in culture, latrunculin A treatment does not affect the kinetics of endocytosis (Li and Murthy, 2001; Sankaranarayanan et al., 2003; Hua et al., 2011), whereas actin reportedly

mediates ultrafast endocytosis in the same preparation (Watanabe et al., 2013). Ultrafast endocytosis is also mediated by actin at cerebellar mossy fiber synapses (Delvendahl et al., 2016). At the calyx of Held and hippocampal synapses, actin is reportedly required for all types of endocytosis (Wu et al., 2016).

1.6 Organization and importance of microtubule network in presynaptic calyceal terminals

Microtubule (MT) is a polymer composed of globular α- and β- tubulin submits, each with MW of ~50 kDa. MT is the second most abundant cytoskeletal protein in the presynaptic terminal next to actin and constitutes ~1.4% of total synaptosomal proteins, with a copy number of 12000 per synapse (Wilhelm et al., 2014). The α/ β-heterodimers are arranged as hollow cylindrical tubes of 24 nm in diameter, conferring stiffness to MTs. Through longitudinal interactions between the ends of adjacent subunits, the heterodimers polymerize in a head-to-tail fashion into a linear protofilament. Through lateral interactions, protofilaments associate side by side into a sheet or cylinder to form a MT. MTs are highly polar structures, because of different polymerization rates at both ends. The end exposing β- tubulin grows faster and is called the plus (+) - end (Mitchison, 1993), while the slower growing exposes α- tubulin and is called the minus (-) - end (Cote and Borisy, 1981). In axons, MTs are uniform in polarity, with (+) - ends being directed from a cell body to an axon terminal, whereas MTs are not uniform in polarity in dendrites (Baas et al., 1988). Both α- and β- subunits are bound to GTP, GTP molecules bound to β-tubulin are hydrolyzed shortly after being incorporated into MTs. This causes a conformational change of tubulin molecules, thereby driving the dynamic behavior of MTs. Rapid MT shrinkage (‘catastrophe’) occurs in combination with polymerization (‘rescue’) causing dynamic instability of MTs (Mitchison and Kirschner, 1984). A variety of microtubule-associated proteins (MAPs) and their post-translational modifications regulate assembly, dynamics, organization and interaction of MTs with other cellular components. MTs play roles in chromosomal separation during cell division,

regulating cell polarity, cell morphogenesis and migration, and intracellular cargo trafficking.

Neuronal MTs were first described by EM studies as fibrillar structures running along the axoplasm and involved in intracellular transport of cargoes from cell body towards axon terminals (Schmitt, 1968). EM studies of neurons derived from lamprey larvae provided the first evidence for the association of SVs and MTs close to synaptic junction but, away from neurotransmitter release zones and without any contact with presynaptic PM (Smith et al., 1970). Initially, tubulin was characterized as a soluble protein in brain homogenates that binds to colchicine (Borisy and Taylor, 1967). Later, this protein was found to constitute 28% of synaptosomal proteins (Feit and Barondes, 1970; Feit et al., 1971; Lagnado et al., 1971). Although the existence of MTs in presynaptic terminals was controversial, as EM studies failed in preserving intact MTs at the presynaptic terminal (Blitz and Fine, 1974; Kadota et al., 1976), a novel protocol of stabilizing MTs revealed their presence in presynaptic compartments. MTs were shown to run through the presynaptic cytoplasm, in close association with SVs and AZ (Gray, 1975; Bird, 1976).

Although MTs are detected in synaptosomes by immunocytochemical studies (Cumming et al., 1983), some immunohistochemical studies argued against it (Matus et al., 1975; Matus et al., 1981). Later, it was suggested that these conflicting observations resulted from different stabilities of MTs at different temperatures (Hajos et al., 1979). At the calyx of Held presynaptic terminals in adult cats, electron tomography (ET) studies indicate that MTs associates with mitochondrion-associated adherens complex, that is thought to contribute to precise positioning of mitochondria within the terminal (Perkins et al., 2010). Similarly, in goldfish retinal bipolar cells, MTs emerged from axon, form loops in presynaptic space, where it interacts with mitochondria. These reports suggest that MTs place mitochondria in presynaptic space to provide sustained energy for continuous neurotransmitter release (Graffe et al., 2015). Immunofluorescence analysis of the

cultured calyceal terminals revealed tubulin-containing polymers that span nearby swellings of presynaptic terminals containing SVs (Guillaud et al., 2017).

Structural and biochemical studies suggest that MTs interact with mitochondria, and also with SVs through synapsins in the presynaptic terminal (Schnapp and Reese, 1982; Nakayama and Silverman, 1986; Hirokawa et al., 1989; Gotow et al., 1991; Perkins et al., 2010). In presynaptic terminals Ca^{2+}- calmodulin kinase (CAMKII) associated with SVs phosphorylates α- and β-tubulins upon stimulation, thereby thought to affect neurotransmitter release (Burke and DeLorenzo, 1981, 1982). Also, another important SV protein, synaptotagmin I interacts with β-tubulin in the presence of Ca^{2+} ions at its C2A and C2B domains. Synaptotagmin I also promotes tubulin polymerization and binds to polymerized tubulin - MTs (Honda et al., 2002). In addition to tubulin and MTs, microtubule-associated protein A and B (MAP 1A and 1B) regulate the surface expression of $Ca_v2.2$ (N-type) in hippocampal and human embryonic kidney 293 cells, respectively (Leenders et al., 2008; Gandini et al., 2014). At *drosophila* NMJ, *drosophila* homolog MAP1B/ Futsch interacts with MTs (Hummel et al., 2000) and controls synaptic growth and bouton formation by regulating synaptic MT cytoskeleton (Roos et al., 2000). Recently, it has been shown that Futsch acts as a link between components of AZ and underlying MT cytoskeleton of the presynaptic terminal, thereby stabilizing the AZ. Furthermore, in Futsch mutants, there is a significant decrease in evoked excitatory junctional currents suggesting the requirement of Futsch for normal neurotransmitter release (Lepicard et al., 2014).

Stabilization of MTs by taxol causes no apparent changes in neurotransmitter release in synaptosomal preparations (Cumming et al., 1983). Also, in another study, it was revealed that intact MTs are required for tetanus toxin-induced blockade of noradrenaline release from synaptosomes (Ashton and Dolly, 1997). These reports indirectly imply the involvement of MTs in neurotransmitter release.

1.7 Scope of the thesis

In this thesis, I first examined how presynaptic actin filaments are involved in SV trafficking and basal synaptic transmission in rodents, before and after hearing onset, using patch clamp recordings and confocal microscopy. I then studied the organization of MTs in calyceal presynaptic terminals using confocal, super-resolution and electron microscopes. Subsequently, I performed functional characterization of MTs in presynaptic terminals using patch clamp whole-cell recordings after pharmacologically disrupting MTs. Finally, I confirmed an involvement of MTs in SV trafficking in cultured calyceal terminals using real-time imaging of fluorescently labeled SVs.

2. MATERIALS AND METHODS

2.1 Ethical approval

All experiments were performed in accordance with guidelines of the Physiological Society of Japan and animal experiment regulations at Okinawa Institute of Science and Technology Graduate University.

2.2 Preparation of acute brainstem slices

I followed the general procedure described by Takahashi (1978) for preparing acute slices from rodents. For obtaining brainstem slices that enable electrophysiological and morphological characterizations of the presynaptic calyx of Held terminals and postsynaptic principal cells in the MNTB region, I followed the procedure described by Forsythe and Barnes-Davies (1993).

Wistar rats of either sex at postnatal day (P) 7-9 (pre-hearing) or 13-16 (post-hearing) were decapitated under deep isofluorane anesthesia and the skull was opened by cutting the skin along the midline from neck to the eye line using scissors. Excess spinal cord and surrounding tissues were removed to expose the skull. Two cuts were made, using fine scissors, near the mouth on either side of the skull and the entire skull was removed to expose dorsal part of the brain. A small spatula was used to retract the brain caudally from the skull. Spring scissors were used to cut the fibers and blood vessels near the brainstem, and isolated brain was transferred to an ice-cold cutting solution (see below for composition). Cooling of tissues slows down the metabolic rate and prevents neurons from anoxia. This step usually takes 1-1.5 min. In the cutting solution, the brain was mounted ventrally and the meninges surrounding the brainstem were removed. A ceramic blade was used to caudally cut the brainstem and cerebellum from the entire brain (Illustration 2). The preparation containing the brainstem and cerebellum was mounted on a Teflon base of a specimen plate, such that the caudal surface is facing upward and the ventral surface facing the cutting blade of the slicer. The mounted preparation was immediately

transferred to a pre-cooled buffer tray and filled with ice-cold and oxygenated cutting solution.

Transverse slices were cut into a thickness of 175-250 µm using a vibrating slicer (VT1200S, Leica) (Takahashi, 1978). Prior to each slicing, the blade angle and amplitude of blade vibration (1.2 mm) were optimized. Initial slicing was performed at a fast blade advancement speed (0.1mm/s). Using the 7th cranial nerve serves as a landmark for the MNTB region, the blade advancement speed was lowered to 0.05 mm/s and slices were collected from this point. The slices containing MNTB region were immediately transferred onto a nylon mesh in a maintenance chamber soaked in oxygenated aCSF (See below for composition). The slices were incubated for 1h at 37º C expecting that neurons recover from cutting damage before experiments.

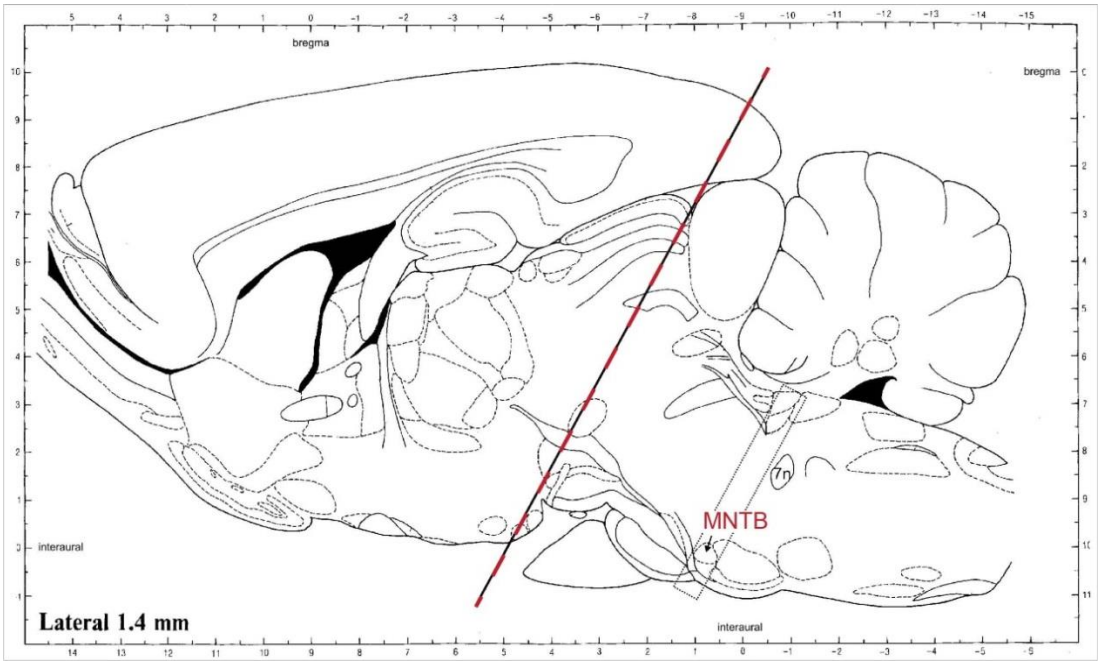

Illustration 2: Lateral view of the adult rat brain.

The diagonal line indicates the cut that was performed to separate the cerebrum from the brainstem. The latter was then mounted for slicing. The region of interest is highlighted by the dashed box and contains the MNTB. While slicing, the seventh cranial nerve (7n) served as a landmark that indicated the beginning of the region of interest. Modified from Paxinos and Watson (1982).

2.3 Solutions

Solution for cutting slices contained (in mM): 200 sucrose, 2.5 KCl, 10 glucose, 1.25 NaH_2PO_4, 2 sodium pyruvate, 3 myo-inositol, 0.5 sodium ascorbate, 26 $NaHCO_3$, 1 trehalose, 6 $MgCl_2$. The cutting solution was kept in -80º C for 10 min and then transferred to -20º C for ~20 min to form a slushy mixture. Then, the solution was kept on ice and bubbled with 95% O_2 and 5% CO_2 during slicing.

Artificial cerebrospinal fluid (aCSF) contained (in mM): 125 NaCl, 2.5 KCl, 1 $MgCl_2$, 2 $CaCl_2$, 10 glucose, 3 myo-inositol, 2 sodium pyruvate, 0.5 sodium ascorbate, 1.25 NaH_2PO_4, 26 $NaHCO_3$ (310-315 mOsm, pH 7.4 when saturated with 95% O_2 and 5% CO_2).

For recording excitatory postsynaptic currents (EPSCs), 10 µM bicuculline methiodide, 0.5 µM strychnine hydrochloride (TCI) were added to the aCSF to block $GABA_A$ receptors, glycine receptors, respectively. In some experiments, the competitive AMPA receptor antagonist kynurenic acid (kyn, 2 mM) was further added to minimize saturation and desensitization of postsynaptic AMPA receptors with neurotransmitter glutamate.

For presynaptic membrane capacitance measurements, the aCSF contained 10 mM tetraethylammonium chloride (TEA-Cl), 0.5 mM 4-aminopyridine to block voltage-gated potassium (K^+) channels (4-AP), 1 µM tetrodotoxin (TTX) to block voltage-gated sodium (Na^+) channels, together with 10 µM bicuculline methiodide and 0.5 µM strychnine hydrochloride.

To disrupt F-actin, latrunculin A was utilized. Stock solution of latrunculin A (20 mM) was stored at -30º C and was dissolved in aCSF to a final concentration of 20 µM. Slices were pre-incubated with latrunculin A for an hour and transferred to the recording chamber. The slices were used up to one hour for patch clamp experiments. To disrupt MTs, vinblastine sulfate was utilized. Stock solution (5 mM) was stored at -30º C and was dissolved in aCSF to a final concentration of 1-50 µM. The slices were

either pre-incubated (for imaging experiments) or bath perfused with vinblastine (for patch-clamp electrophysiological recordings).

For EPSC recordings, the postsynaptic pipette solution contained (mM): 125 CsF, 30 CsCl, 10 HEPES, 5 EGTA, 1 $MgCl_2$, 5 QX314-Cl. The pH and osmolarity was adjusted to 7.3-7.4 (with CsOH) and 305-310 mOsm, respectively. For capacitance measurements, the presynaptic pipette solution contained (mM): 126 methanesulfonate, 30 CsCl, 10 HEPES, 0.5 EGTA, 12 disodium phosphocreatinine, 3 Mg-ATP, 1 $MgCl_2$. The pH and osmolarity was adjusted to 7.3-7.4 (with CsOH) and 315-320 mOsm, respectively.

2.4 Visual identification of the calyx of held in slices

After incubation for 1 h at 37º C, slices were transferred to a recording chamber with a cover glass bottom. The recording chamber was equipped with an inlet port for incoming solutions that bathed the slices and an outlet port connected to a suction pump that removes the solutions. The recording chamber was connected to a peristaltic pump (Dynamax RP-1, Rainin instrument co.) with adjustable flow rate. The tube connected to the pump was warmed to near PT (Temperature Controller TC-344C, Harvard Apparatus). Perfusates were also kept at PT using another heater connected to the platform of the microscope stage. Slices were immobilized in the recording chamber using a U-shaped platinum grid with nylon wires running in parallel (Edwards et al., 1989). All electrophysiological data were recorded using EPC-10/2 patch-clamp amplifier (HEKA) equipped with Patch-master software (HEKA).

Slices were immobilized in the recording chamber placed on the platform of a stage-fixed upright microscope (BX51WI, Olympus) optimized for simultaneous differential interference contrast views of cells and pipettes (Takahashi, 1978). The calyx of Held presynaptic terminals and postsynaptic MNTB principal cells were visually identified with a 40X water immersion objective (LUMPLFLN 40XW, 0.8 N.A, Olympus). Images were acquired using a monochrome digital CCD camera (AxioCam MRm, Carl Zeiss) controlled by a software (Zen Lite 2, Blue edition,

Carl Zeiss). For manipulations, cells were viewed on a monitor (FlexScan M1900-R, Eizo, Japan).

2.5 Patch-clamp whole-cell recordings

Electrodes for patch-clamp recording were made from borosilicate glass with a filament (1.5 mm outer and 0.86 mm inner diameter from Harvard Apparatus) using a temperature controlled horizontal micropipette puller (Sutter Instrument). For recording from postsynaptic principal cells, pipettes with a larger tip diameter and low resistance (1-3 MΩ) were used, whereas pipettes of smaller diameter and higher resistance (4-5 MΩ) were utilized for recording from presynaptic calyceal terminals. Pipette and cell capacitances were compensated using a built-in compensation circuitry. The series resistances (Rs) were 4-7 MΩ for postsynaptic recording and 8-14 MΩ for presynaptic recording and were compensated up to 60% for final value to be ~ 3 MΩ and ~ 7 MΩ, respectively. Data were acquired at a sampling rate of 50 kHz (for synaptic currents) or 100 kHz (for capacitance measurements) after low-pass filtering (Bessel, 5 Hz corner frequency).

Excitatory postsynaptic currents (EPSCs) were evoked in the principal neurons of MNTB region by afferent fiber stimulation using a custom-made bipolar tungsten electrode. The bipolar electrode was placed on the halfway between the midline and MNTB region to stimulate axonal bundles projecting from aVCN. For the whole-cell recording of evoked EPSCs, principal neurons were voltage-clamped at -70 mV.

The short-term synaptic depression (STD) was induced by a train of 30 stimuli at 100 Hz (or 300 Hz) followed by test stimuli after different inter-stimulus intervals (ISI, 0.02-10 s). The amplitudes of EPSCs recorded during the train and after the test stimuli were used to measure various parameters involved in synaptic transmission.

For recording spontaneous EPSCs that are equivalent to the miniature (m) EPSCs at the calyx of Held with single presynaptic input (Sahara and Takahashi,

2001; Ishikawa et al., 2002), the principal cells were voltage-clamped at -70 mV. The postsynaptic series resistances were not compensated and aCSF did not contain kyn or TTX.

The amplitude of evoked EPSCs was measured and analyzed using a custom-made macro in Igor (IGOR Pro 6.22; Wavemetrics). The software automatically measures the peak amplitudes of individual EPSCs and estimates their (10-90) % rise time during a train (100 or 300 Hz). The decay time constants of EPSCs were measured manually after double-exponential fitting. The EPSC amplitudes during the train and after test stimuli were used to estimate % recovery at different ISIs. The rate of recovery of EPSCs from synaptic depression was computed from % recovery after different ISIs after fitting recovery time course with double exponential function, from which fast (τ_f) and slow (τ_s) time constants and their relative amplitudes (A_f, A_s) were determined. The weighted mean time constant (τ_m) was calculated from the following equation: $\tau_m = Af*\tau_f + A_s*\tau_s$

The estimation of the RRP size (Nq) and release probability (p) was based on the quantum hypothesis of neurotransmission (Del Castillo and Katz, 1954; Sahara and Takahashi, 2001) and assuming that the depression is primarily caused by depletion of vesicles in RRP and also that release probability remains constant during stimulation. Based on these assumptions, the RRP size was estimated from the zero-time intercept of a line fitted to the cumulative amplitude plot of EPSCs (Schneggenburger et al., 1999). The p value was determined by dividing the amplitude of first EPSC (Npq) in the train by RRP size.

Spontaneous mEPSCs were analyzed off-line using AxoGraph (Axon Instruments). Initially, a mEPSC template was constructed for each cell, by averaging 30 - 150 mEPSCs. Then, spontaneous events having a similar waveform were selected after optimal scaling. Only those events >3 times larger than the background noise (2-4 pA in standard deviation) were adopted for further analysis. Overlapping mEPSCs were excluded from analysis upon visual inspection. The selected events were averaged to compute the amplitude, rise time and decay time kinetic of mEPSCs.

Presynaptic release rates were calculated by deconvolution of eEPSCs with mEPSCs. This method is based on the assumptions that eEPSCs are a linear summation of mEPSCs and that each mEPSC corresponds to single presynaptic fusion event. However, in the calyx of Held with around 550 AZs and around 5-6 releasable vesicles in each AZ, simple deconvolution analysis cannot be applied directly. Strong stimulation would lead to excess glutamate in the synaptic cleft, which would be detected postsynaptically, yet doesn't correspond to additional release. This "spill-over current" caused by delayed transmitter clearance from the synaptic cleft must be subtracted from compound EPSC prior to estimation of presynaptic release rates. Additionally, postsynaptic receptor saturation and desensitization that would lead to changes in mEPSCs during prolonged stimulation were counteracted pharmacologically using kynurenic acid as mentioned previously. The release rates were estimated by adopting the deconvolution method by Neher and Sakaba (Neher and Sakaba, 2001; Sakaba and Neher, 2001b). This method incorporates a simple model of glutamate diffusion to estimate the size of residual current into deconvolution algorithm. The analysis was implemented in Igor Pro. The parameters for mEPSC kinetics and spill-over current were then adjusted manually so that the spill-over current accounted for the decay phases of the eEPSCs. The resulting estimate for the spill-over current was then subtracted from the eEPSCs. Deconvolution with the mEPSC then yielded the quantal release rate.

Membrane capacitance changes in presynaptic terminal reflect the fusion of SVs (exocytosis) and retrieval of SVs (endocytosis) with a corresponding increase and decrease in membrane surface area respectively. The capacitance measurements from the presynaptic calyceal terminals were made at PT after establishing whole-cell configuration (Yamashita et al., 2010). The presynaptic calyceal terminals were voltage-clamped at a holding potential of -80 mV and a sinusoidal voltage command (1 kHz, 60 mV in peak-to-peak amplitude) was applied. A single step pulse to + 10 mV was applied for 20 ms to induce presynaptic Ca^{2+} currents (I_{ca}). The recording pipette was coated with dental wax to reduce pipette capacitance.

Membrane capacitance changes (ΔC_m) within the first 450 ms of the depolarizing step pulse were excluded from analysis to avoid contamination due to

conductance-dependent capacitance artifacts (Yamashita et al., 2005). To avoid the influence of capacitance drift on the baseline, we discarded data when the baseline drift measured 0-10s before stimulation was > 5fF/s. When the baseline drift was between 1-5 fF/s, we subtracted a linear regression line of the baseline from data for baseline correction. The intra- and extracellular solutions for capacitance measurements were used as described previously (See above for composition).

2.6 Imaging studies

2.6.1 Antibodies

Following primary antibodies were used for experiments; anti-VGLUT1 guinea pig antiserum (1:2000; AB5905; Millipore) and anti-synaptophysin rabbit polyclonal antiserum (1:250; catalog #101002; Synaptic Systems) for observing SVs and anti-α-tubulin mouse monoclonal clone DM1A (1:250; catalog #T9026; Sigma-Aldrich), anti-β-tubulin III rabbit (1:1000; product #2200; Sigma-Aldrich) for observing tubulin. The secondary antibodies were goat IgG conjugated with AlexaFluor -488, -568, or -647 (1:400; Invitrogen).

2.6.2 Preparation of tissue for imaging

Acute brainstem slices (250 µm) were cut (see above) and fixed with 4% paraformaldehyde (PFA) in phosphate buffer saline (PBS) overnight at 4°C. On the following day, slices were rinsed 3 times in PBS, permeabilized in PBS containing 0.5% Triton X-100 (Tx-100; Nacalai Tesque) for 30 min at PT and blocked in PBS containing 3% bovine serum albumin (BSA, Sigma) and 0.05% Tx-100 for 45 min at PT. Slices were incubated overnight at 4°C with primary antibody diluted in PBS 0.05% Tx-100, 0.3% BSA. On the next day, slices were rinsed 3 times with PBS containing 0.05% Tx-100 for 10 min at PT and incubated with corresponding secondary antibody diluted in PBS 0.05% Tx-100, 0.3% BSA for 1h at PT. Slices were further rinsed 3 times in PBS 0.05% Tx-100 for 10 min at PT, and a final wash in PBS for another 10 min at PT. Before mounting, the nucleus was stained with NucBlue (Life Technologies, USA) in PBS for 20 min at PT according to manufacturer's instruction. Slices were then directly mounted on glass slides

(Matsunami Ind., Ltd; USA) using a mounting medium (Ibidi GmbH; Germany) and sealed using a nail polish.

For Stimulated Emission Depletion (STED) microscopy, slices were sequentially incubated in PBS containing 10, 20 and 50% of 2,2'-thiodiethanol (TDE) for up to 1 h each, followed by three times in 97 % TDE solution for 10 min each, and mounted on glass slides using TDE mounting reagent (Abberior GmBH, Germany).

2.6.3 Image acquisition and analysis

Confocal images were acquired on a Laser Scanning Microscope (LSM 780, Carl Zeiss MicroImaging GmBH, Germany) equipped with a Plan-Apochromat 63x, oil immersion objective with a numerical aperture (NA) of 1.4 and excitation laser lines (wavelength, 405nm, 488nm and 561nm). Super-resolution imaging was performed on STED microscope (TCS SP8, Leica) 3X equipped with a HC PL APO CS2 100x, 1.4 NA oil immersion objective (Leica) and a tunable white laser excitation line and depletion laser lines (wavelength, 592 nm, 660 nm and 775 nm).

The confocal images were processed in Zen Lite 2 (Black or blue edition, Carl Zeiss). For quantifying fluorescence intensity levels, the region of interest was delimited to calyceal terminals and the background fluorescence was subtracted in ImageJ software (NIH, USA). STED images were deconvoluted in Huygens software (Leica Microsystems K.K, Japan) to increase the signal-to-noise ratio and image resolution and further processed in Leica Las AF Lite software (Leica Microsystems K.K).

2.6.4 Live imaging of SiR-tubulin stained slices and SiR-actin staining in HeLa cells

To label microtubule network, acute brainstem slices (250 µm) were incubated with SiR-tubulin (1µM; Cytoskeleton, inc., Switzerland) at 37°C according to manufacturer's instructions. SiR-tubulin is a cell-permeable, live cell imaging fluorogenic probe, which stains endogenous MTs at docletaxel binding sites. Slices

were mounted onto a 35 mm ibidi dish and immobilized using a platinum grid holder. ACSF with or without 50 µM vinblastine was perfused at 37°C and SiR-tubulin fluorescence was monitored in real time using a laser scanning confocal microscope (LSM 780) with an airyscan module (Carl Zeiss). To label actin and microtubule network, HeLa cell cultures were incubated with SiR-actin (1µM; Cytoskeleton, inc., Switzerland) or SiR-tubulin at 37°C according to manufacturer's instructions. SiR-actin, similar to SiR-tubulin is a cell-permeable, live cell imaging fluorogenic probe, which stains endogenous F-actin at jasplakinolide binding sites.

2.6.5 Primary neuronal cultures

Primary cultures of calyceal terminals were established as described previously (Dimitrov et al., 2016; Dimitrov et al., 2018). In short, mouse brains from E18 to P1 pups were removed and the CN and MNTB regions were microdissected in ice-cold Hank's balanced salt solution and dissociated using nerve cell dissociation medium. Dissociated neurons were plated in poly-D-lysine pre-coated dishes to a final density of 1.6-1.8 x 10^5cells per 35 mm culture dish and supplemented with growth factors as previously described (Dimitrov et al., 2016).

2.6.6 Synaptic vesicle labeling and live imaging

To detect SVs in calyceal terminals, SVs were labeled with rabbit polyclonal antibodies directed against the luminal domain of synaptotagmin-2 tagged with quantum dots Q655 as previously described (Guillaud et al., 2017). Before imaging, the culture medium was replaced and perfused with standard Tyrode's salt solution (pH = 7.4) maintained at 37 ºC and observed on LSM 780.

2.6.7 Image analysis and vesicle tracking

To analyze the movements of SVs, fluorescent spot detection and tracking on 30 s time series were performed as previously described (Guillaud et al., 2017). In short, IMARIS 8.1 tracking software with Measurement Pro and Vantage plugins (Bitplane, Switzerland) was used to obtain information about vesicle trajectories (i.e. trajectory length).

2.7 Electron microscopic studies

The ultrastructure of the calyceal presynaptic terminals was observed using transmission electron microscopy (TEM). A 1mm block of transverse brainstem slice containing the MNTB regions was made as described above. Slices were immediately immersed into pre-warmed 20% BSA solution in aCSF for 5 min. Excess albumin was removed by washing with aCSF. The slice was immediately fixed using 2.5% glutaraldehyde in 0.1 M cacodylate buffer for 1h at PT. Once the tissue was fixed, I excised MNTB regions from the slice. The samples were washed by aspiration for 3 × 5 min in 0.1M cacodylate buffer. After washing, the samples were post-fixed in 1% osmium tetroxide (OsO_4) in 0.1M cacodylate buffer for 1 h. After post-fixation, the samples were washed with pure water 3 x 5 min. For dehydration, the sample was sequentially immersed in 70%, 80 %, 90%, 95%, 100%, 100%, 100% ethanol for about 5 min each and decanted. The samples were treated with epon 812 and ethanol in 1:1 ratio for 30 min. After which samples were embedded with just pure epon 812 and left in a vacuum chamber for 1 h. The vacuum was turned off after 1 h and samples were left in the chamber overnight. On the next day, a drop of pure epon was placed in numbered polyethylene capsules and the sample was transferred into appropriate capsules. The capsules were cured for 48 h in a 60° C oven. Initially, slices of > 1µm thickness were made using a diamond knife in an ultra-microtome (EM UC6, Leica) to trim before reaching the area of interest. Upon reaching the area of interest, 70 nm thick sections were made and placed on grids. The grids were air-dried for 10 min and then the samples were post-stained. For post-staining, the grids were immersed in 4% uranyl acetate for 30 min and washed with pure water and then with lead citrate for 10 min. The samples were finally washed and air-dried before observation in TEM. The samples were observed in Jeol JEM-1230R (Jeol; Japan) TEM operating at 100 keV.

2.8 Statistical analysis

The electrophysiological data were analyzed using IGOR Pro 6.22 (Wavemetrics), MS Excel 2010 (Microsoft), Origin Pro 8.6 (Origin labs) and imaging data were

analyzed using Las AF Lite (Leica) and Image J. All values are given as mean ± SEM, and $p < 0.05$ was taken as a significant difference in Student's unpaired t-test.

3. RESULTS

As an initial part of my thesis work, I studied the involvement of actin filaments in SV trafficking in both pre- and post-hearing rats. The results are summarized below; all the experiments pertaining to actin filaments were performed at RT to allow direct comparison with previous reports.

3.1 Role of actin filaments in the calyx of Held presynaptic terminals of pre-hearing rats

To examine the role of actin filaments in synaptic transmission, I tested the effect of latrunculin A (20 µM, 1 h incubation at RT) on nerve-evoked EPSCs at the calyx of Held. In P7-9 rats before hearing onset (~P13), neither mean amplitude nor rise time (10-90%) of EPSCs was affected by latrunculin A treatment, whereas decay times were prolonged (Figure 1A, B). Using the repetitive stimulation protocol (see Materials and Methods), I evaluated the effect of latrunculin A on RRP size (Nq) and release probability (Pr). Latrunculin A treatment had no effect on these parameters (Figure 2), but it significantly slowed the time course of recovery from synaptic depression induced by a train of 30 stimuli at 100 Hz. These results confirm the previous report at the calyx of Held in pre-hearing rats (Sakaba and Neher, 2003), suggesting that actin filaments are involved in RRP replenishment after SV depletion (Figure 3).

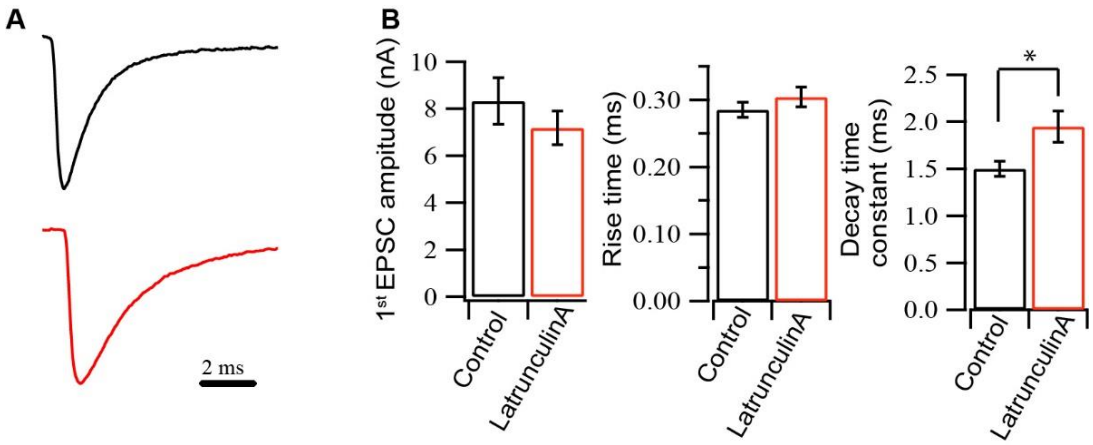

Figure 1: Latrunculin A treatment prolongs decay time constant of EPSCs in pre-hearing rats

A. Representative traces of normalized evoked EPSCs in control (black) and latrunculin A (red) treated conditions recorded at RT.

B. Bar graphs summarize the effect of latrunculin A on EPSC amplitude (1^{st}), rise time and decay time constants of evoked EPSCs in control (n = 6) and latrunculin A (n = 5) treated conditions. (*$p<0.05$).

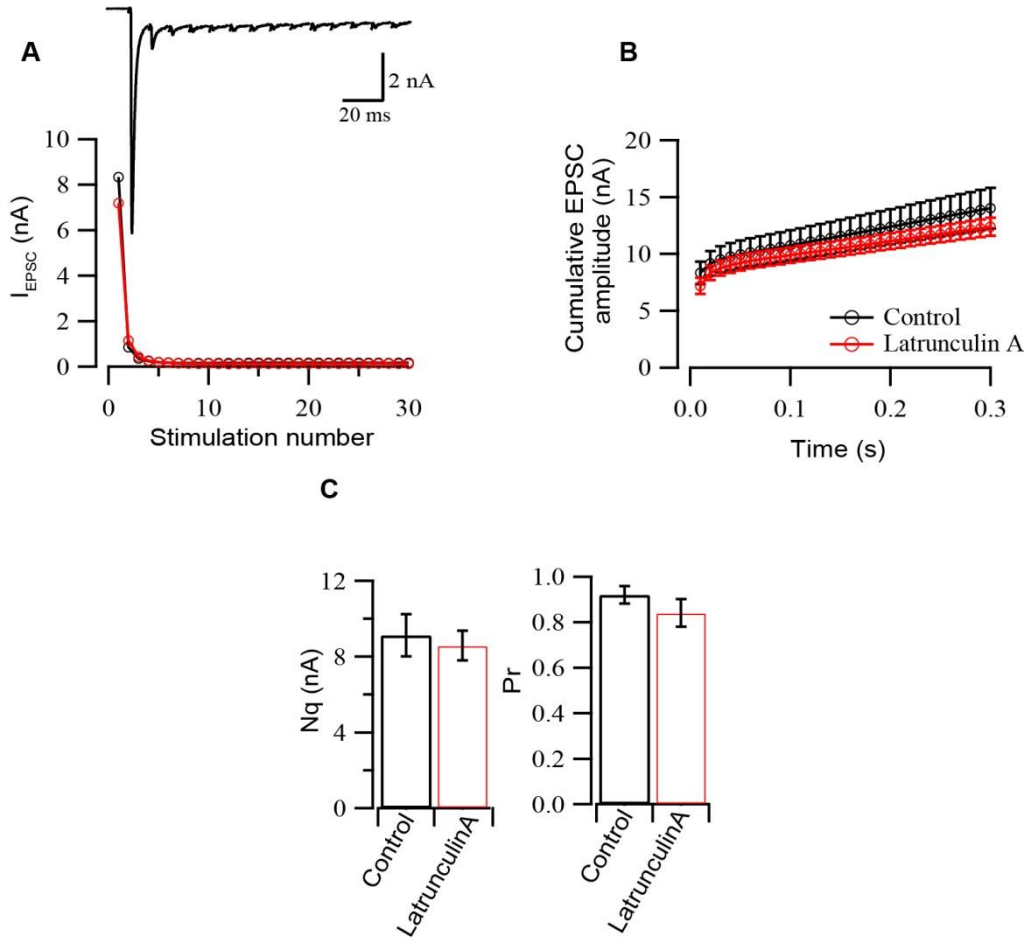

Figure 2: Latrunculin A treatment doesn't affect RRP size (Nq) or release probability (Pr)

A. *Upper panel*. Sample trace is the 1st to 14th EPSCs during the train in control at RT.

   Lower panel. EPSC amplitudes during a train of 30 stimuli at 100 Hz in control (black, n = 6) and latrunculin A treated condition (red, n = 5).

B. Cumulative EPSC amplitudes during a 100 Hz train in control (black) and latrunculin A treated condition (red).

C. Bar graph summary of mean Nq and Pr in control (n = 6) and latrunculin A treated condition (n = 5).

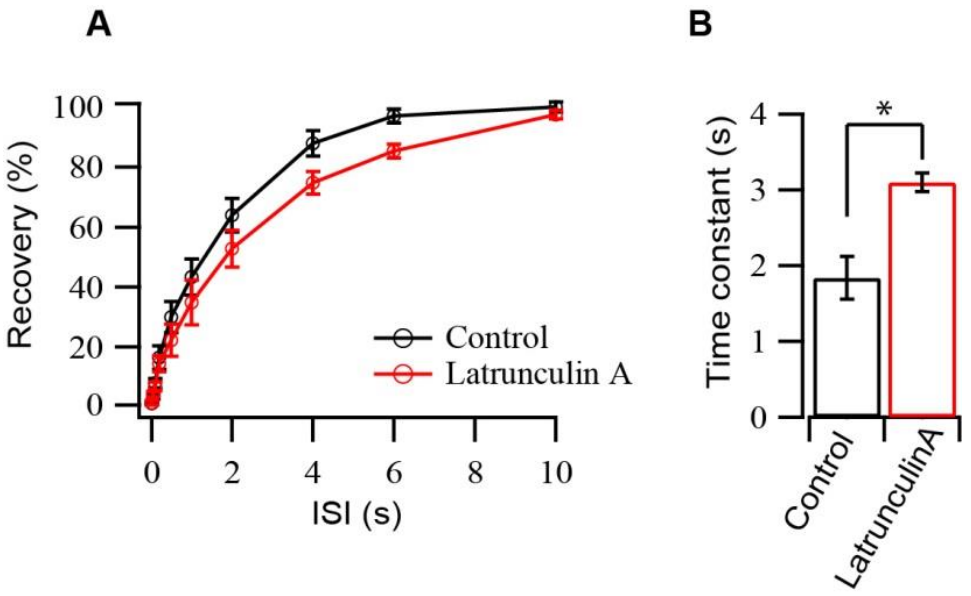

Figure 3: Latrunculin A treatment prolongs recovery time constant of EPSCs from STD in pre-hearing rats

A. Time courses of recovery from STD induced by 30 stimuli at 100 Hz in control (black) and latrunculin A treated (red) slices. Data from both conditions were fitted by a single exponential function (continuous lines).

B. Bar graph summarizes the mean time constants of recovery in both control (n = 6) and latrunculin A treated (n = 5) conditions (*$p<0.05$).

3.2 Role of actin filaments in the calyx of Held presynaptic terminals of post-hearing rats

I next examined whether the effects of latrunculin A on synaptic properties in pre-hearing rats (Figures 1-3) persist after hearing onset in post-hearing rats. Like in pre-hearing rats, latrunculin A treatment prolonged the decay time of evoked EPSCs, but had no effect on their amplitude and rise time (Figure 4A, B). The RRP size and Pr remained unchanged after latrunculin A treatment as in pre-hearing rats (Figure 5B, C). However, latrunculin A treatment no longer affected the rate of recovery from STD at calyces in post-hearing rats (Figure 6A, B). These results suggest that actin filaments become uninvolved in SV replenishment after hearing onset.

In post-hearing rat calyces, I further examined whether latrunculin A affects asynchronous transmitter release or quantal size. At calyces of Held, with single excitatory fiber input, spontaneous EPSCs are equivalent to quantal, or miniature (m) EPSCs (Sahara and Takahashi, 2001; Ishikawa et al., 2002). Like at other synapses (Morales et al., 2000; Meng et al., 2002), latrunculin A significantly increased the mean frequency of mEPSCs (Figure 7, right) but had no effect on their amplitude (quantal size) or kinetics (Figure 7A, B).

Using immunofluorescence staining, I confirmed previous report (Saitoh et al., 2001) that F-actin is present in post-hearing rat calyceal terminals (Figure 8A, B). To ensure that latrunculin A treatment (20 μM, 60 min) effectively disrupts actin filaments, I performed real-time imaging of actin filament using SiR-actin in HeLa cells (Figure 9A). Actin fluorescence intensity decreased during incubation with latrunculin A (20 μM) and became markedly faint 60 min after application. For a control, I incubated HeLa cells with the MT-disrupting drug, vinblastine (50 μM). Vinblastine had no effect on SiR-actin signals (Figure 9C), indicating that the decline of SiR-actin signal caused by latrunculin A, rather than time-dependent fluorescence bleach. The effect of vinblastine was specific to MTs since it disrupted SiR-tubulin signals with time after incubation (Figure 9B) with no effect on SiR-actin signal intensity.

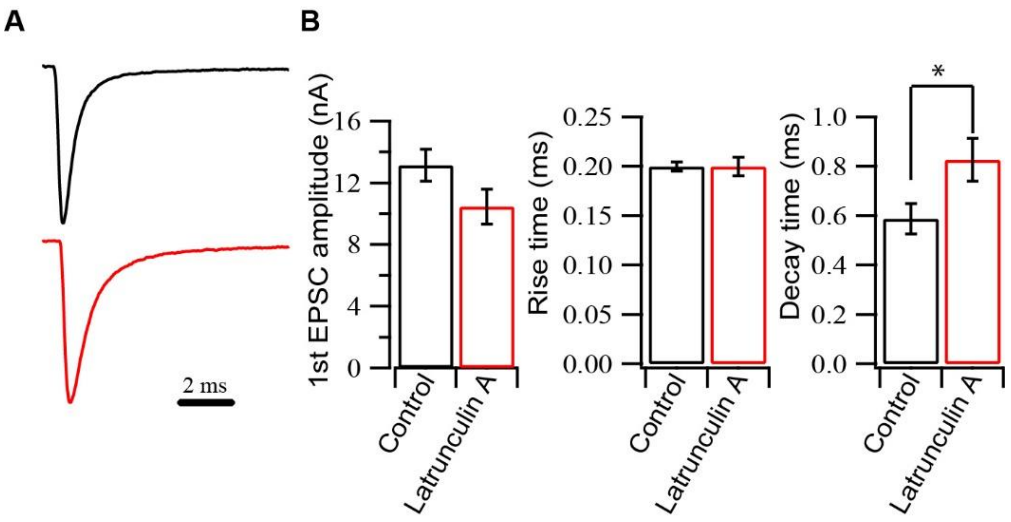

Figure 4: Latrunculin A treatment prolongs decay time constant of EPSCs in post-hearing rats

A. Representative traces of normalized evoked EPSCs in control (black) and latrunculin A (red) treated conditions recorded at RT.

B. Bar graphs summarizing the effect of latrunculin A on EPSC amplitude (1^{st}), rise time and decay time constants of evoked EPSCs in control (n = 7) and latrunculin A (n = 7) treated conditions (*p<0.05).

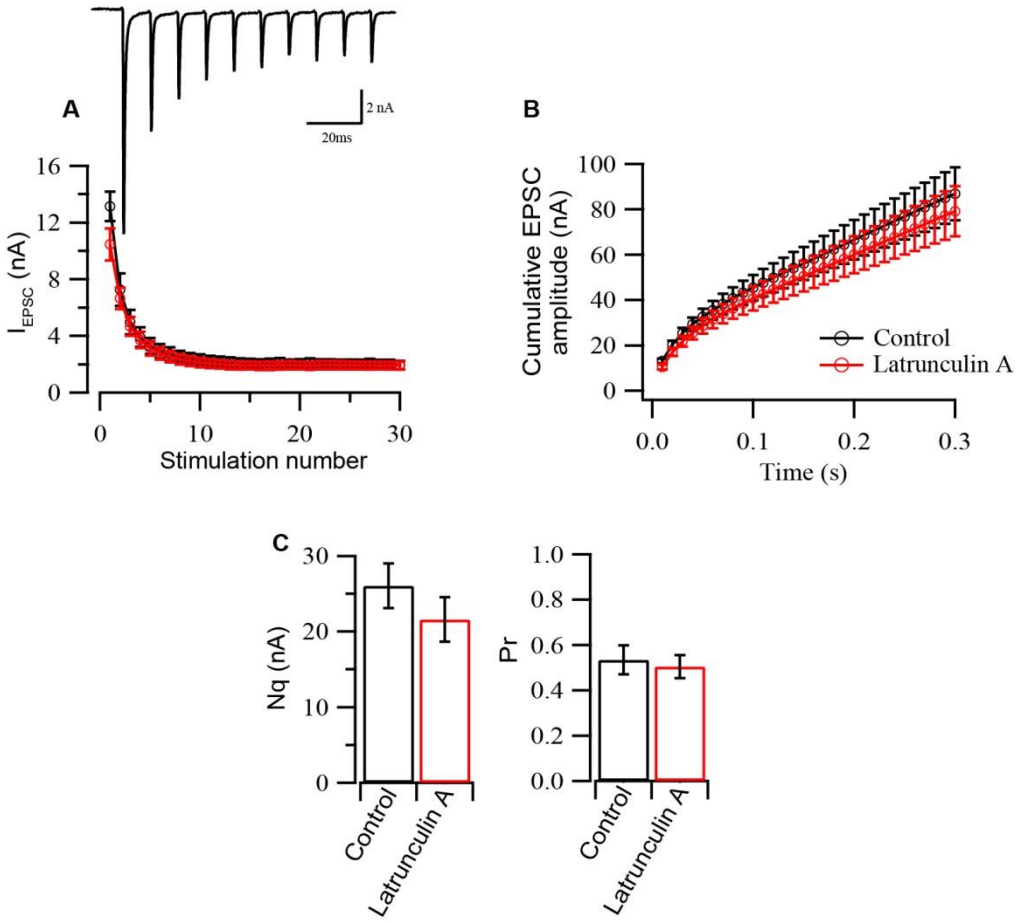

Figure 5: Latrunculin A treatment does't affect RRP size (Nq) or release probability in post-hearing rats

A. *Upper panel.* Sample trace is the 1st to 10th EPSCs during the train in control condition recorded at RT.

   Lower panel. EPSC amplitudes during a train of 30 stimuli at 100 Hz in control (black, n = 7) and latrunculin A treated condition (red, n = 7).

B. Cumulative EPSC amplitudes during a 100 Hz train in control (black) and latrunculin A treated condition (red).

C. Bar graph summary of mean Nq and Pr in control (n = 7) and latrunculin A treated condition (n = 7).

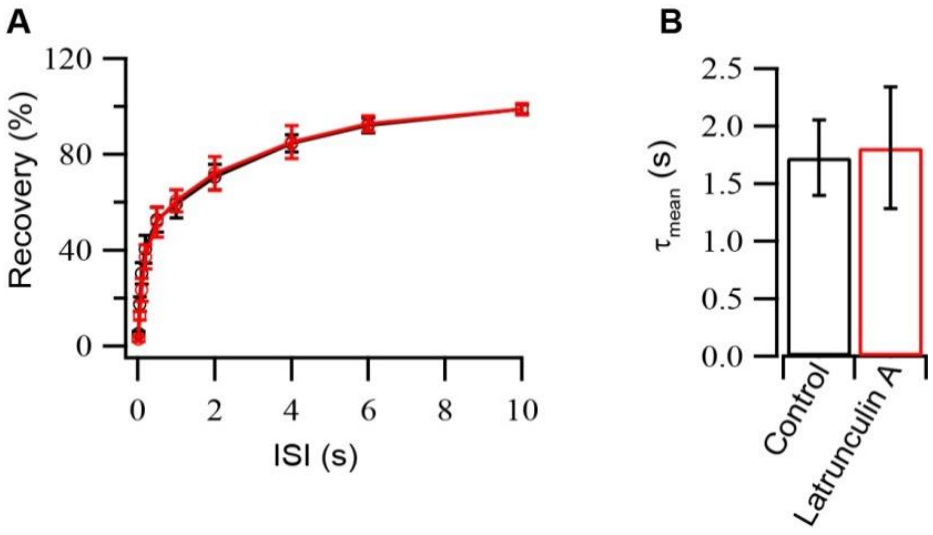

Figure 6: Latrunculin A preincubation doesn't affect rate of recovery of EPSCs from STD

A. Time courses of recovery of EPSCs from depression induced by 30 stimuli at 100 Hz in control (black) and latrunculin A treated condition (red) recorded at RT.

B. Bar graph summary of mean time constants of recovery in control (n = 7) and latrunculin A (n = 7) conditions.

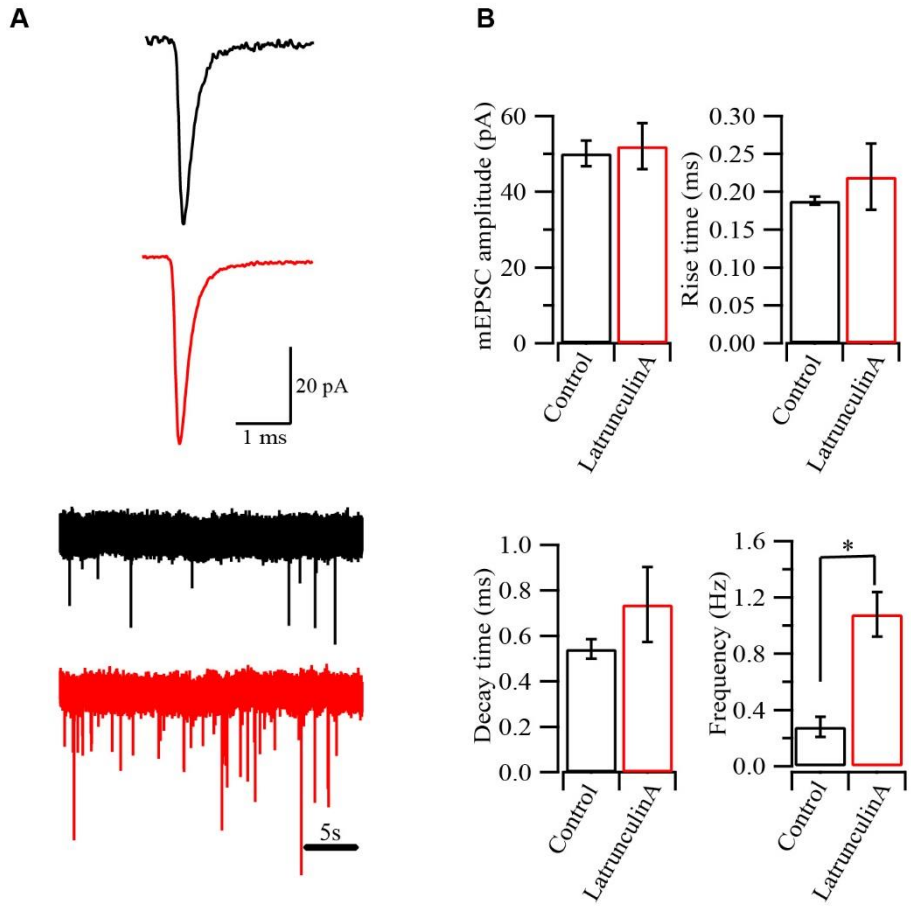

Figure 7: Latrunculin A treatment increases frequency of mEPSC in post-hearing rats

A. Sample mEPSC in control (black) and latrunculin A (red) treated conditions. Sample mEPSC traces in control (black) and latrunculin A (red) treated conditions recorded at RT.

B. Summary bar graphs comparing mEPSC amplitude, rise time, decay time constant and frequency of mEPSC between control (n = 7) and latrunculin A (n = 5) treated conditions.

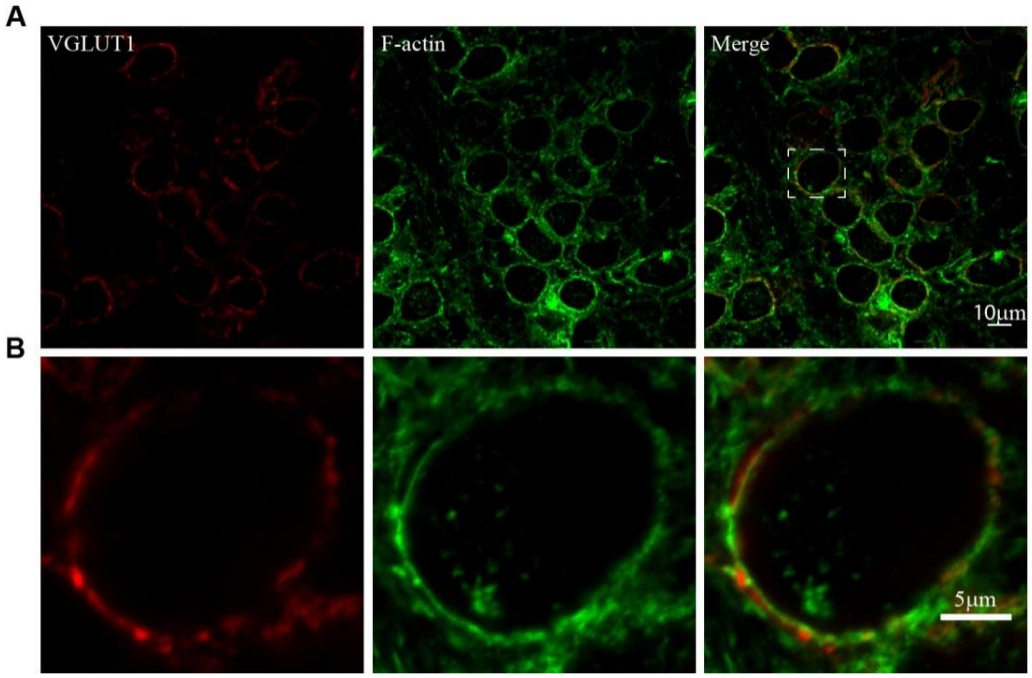

Figure 8: F-actin staining in the calyx of Held presynaptic terminals in acute brainstem slices in post hearing rats

A. Low magnification confocal optical images of VGLUT1 (red) and F-actin (green) immunofluorescence staining in a calyx of Held presynaptic terminal in a brainstem slice from P13 rats.
B. High magnification confocal image of a single calyx of Held terminal (dotted square shown in merge).

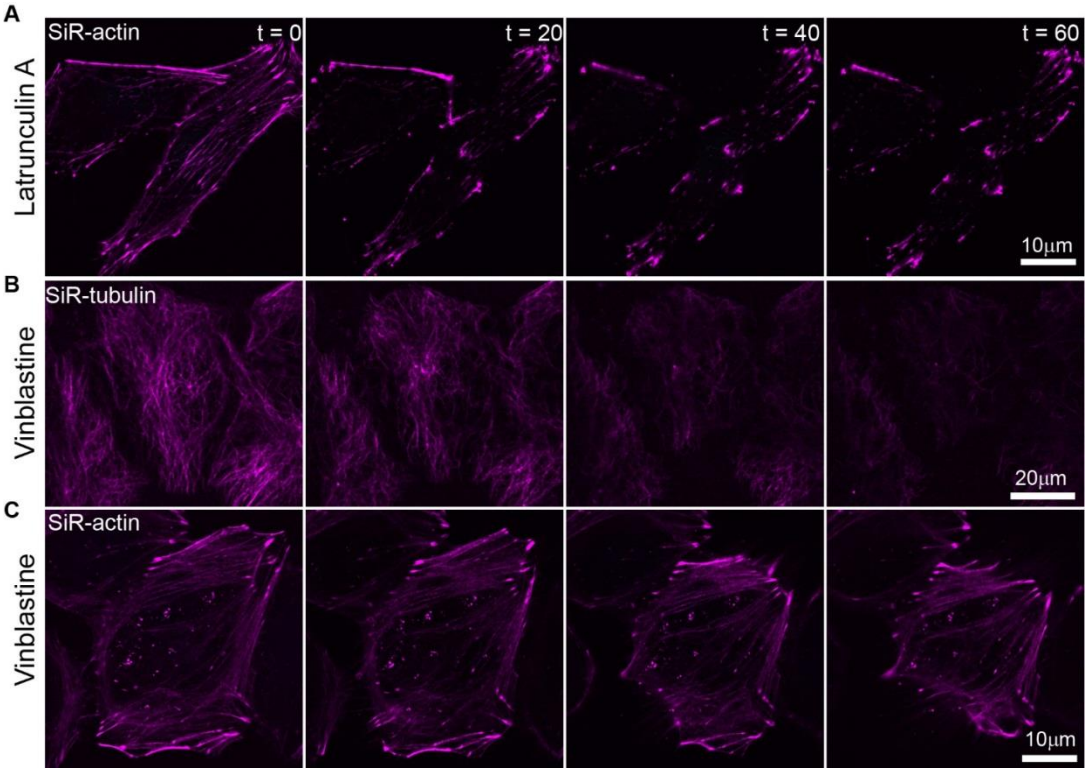

Figure 9: Vinblastine treatment specifically affects MTs but, not actin filaments.

A. Live staining of actin with SiR-actin in HeLa cells and treatment with latrunculin A (20 µM). Sample images show maximum projection of SiR-actin fluorescence in a HeLa cell at varying time points in drug (t = 0 to 60 min).
B. Live staining of MTs with SiR-tubulin in HeLa cells and treatment with vinblastine (50 µM). Sample images show maximum projection of SiR-tubulin fluorescence in HeLa cells at varying time points in drug (t = 0 to 60 min).
C. Live staining of actin with SiR-actin in HeLa cells and treatment with vinblastine (50 µM). Sample images show maximum projection of SiR-actin fluorescence in a HeLa cell at varying time points in drug (t = 0 to 60 min).

Although MTs are likely present in presynaptic terminals, their functional roles remain open. I have made use of the giant calyx of Held presynaptic terminal to gain insight into some functional implications of presynaptic MTs. As MTs are ubiquitous, their genetic deletion or mutation would be lethal for the organism. In this regard, I have employed acute pharmacological disruption to study the functional significance of MTs. In the following sections, I demonstrate results of presynaptic MT cytoskeleton based on morphological and functional observations in the calyx of Held terminals. All the experiments pertaining to MTs were performed at PT (35-36º C).

3.3 Distribution of microtubules in presynaptic calyceal terminals

To visualize the organization of MTs in the calyx of Held presynaptic terminals, we performed tubulin immunostaining in transverse brainstem slices from rats after hearing onset (P13-P15) using specific antibodies against α- or β-tubulin (Figure 10). Tubulin immunoreactivities (i.r.s) were found in presynaptic calyceal terminals surrounding principal neurons in the MNTB. In confocal optical images, tubulin co-localized with the SV protein VGLUT1 (Figure 10A, B). In images obtained using STED microscope, MTs running along axons enter calyceal terminals and branch along presynaptic terminals (Figure 11A, B). At higher magnifications, MTs were found co-localized closely with SVs labeled with VGLUT1 in presynaptic terminal swellings. SVs were found interspersed and clustered at the end of MTs inside the swellings (Figure 12A, B). Also, MTs were found juxtaposed to SVs in finger-like terminal structures, which connect swellings (Figure 13). These results confirm that MTs are present in the calyx of Held presynaptic terminals in close localization with SVs. The EM ultrastructural examinations revealed MTs close to AZ, SVs or mitochondria (Figure 14A, B).

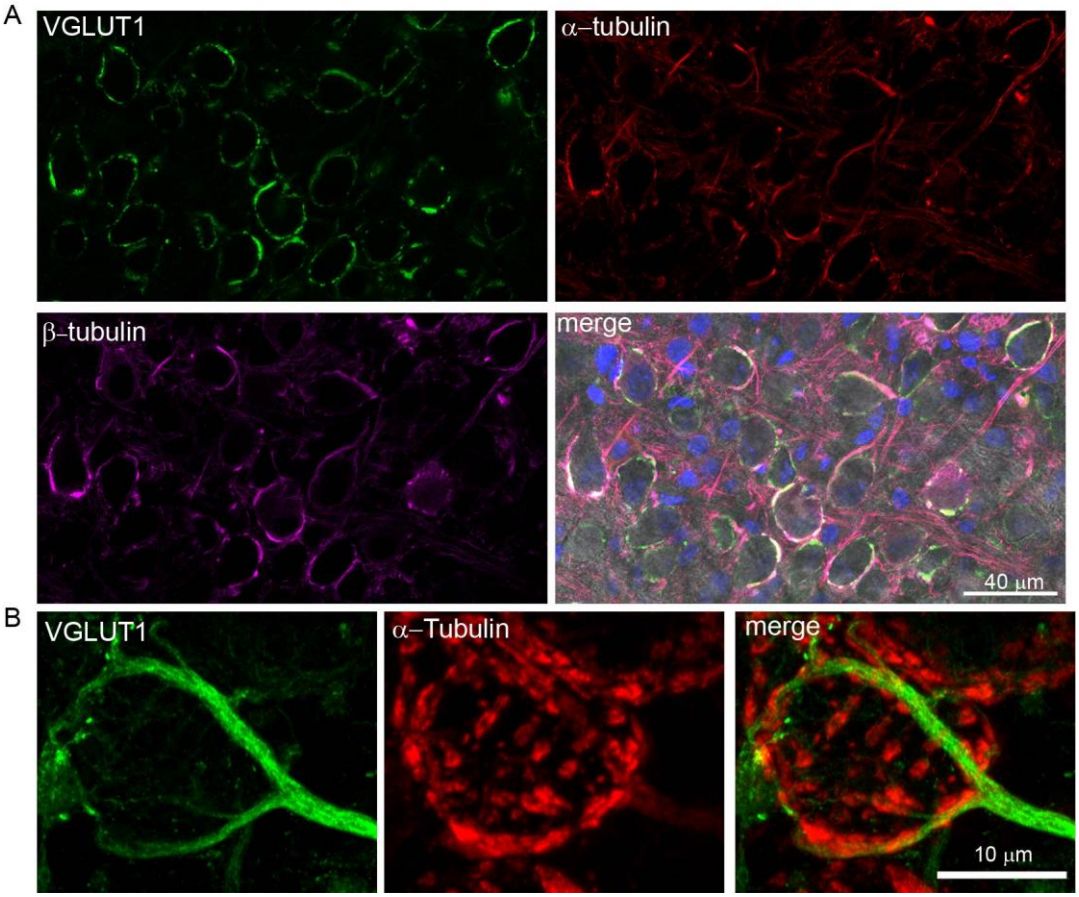

Figure 10: Distribution of microtubules in the calyx of Held presynaptic terminals

A. Low-magnification confocal images of VGLUT1 (green), α-tubulin (red), β-tubulin (magenta) immunofluorescence staining in calyx of Held presynaptic terminals in a brainstem slice from P13 rat.
B. High- magnification confocal images of VGLUT1 (green) and α-tubulin (red) immunofluorescence in a calyx terminal.

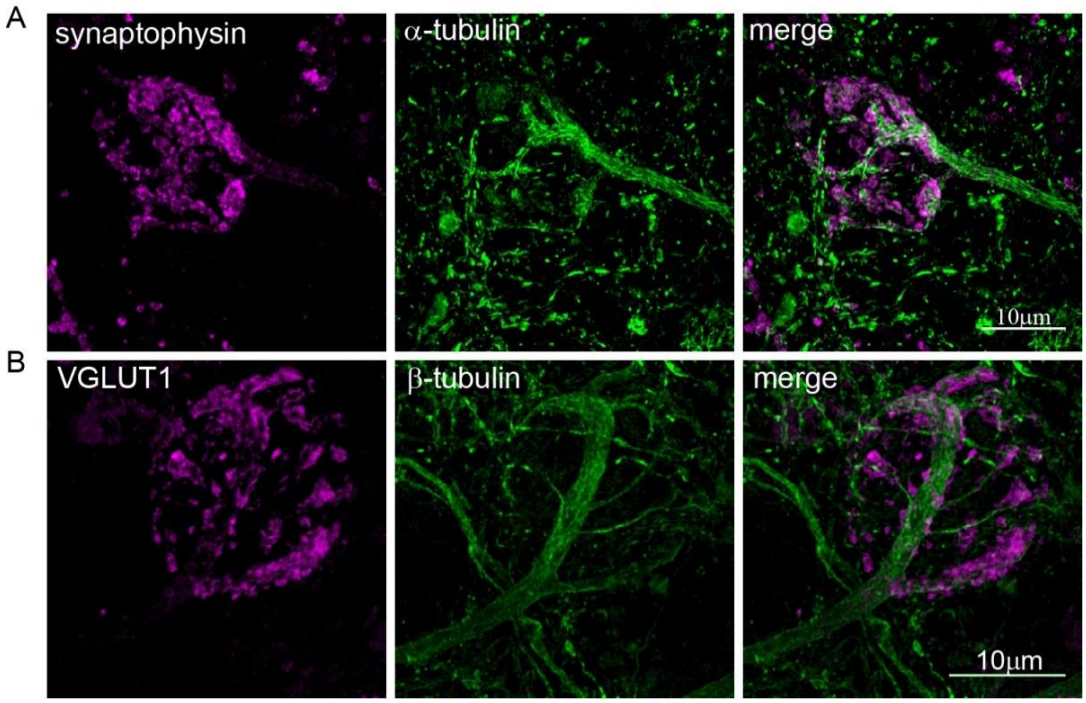

Figure 11: Distribution of MTs in calyx of Held presynaptic terminals viewed using STED microscopy

A. High-resolution STED images of synaptophysin (magenta) and α-tubulin (green) immunofluorescence in a calyx terminal.
B. High-resolution STED images of VGLUT1 (magenta) and β-tubulin (green) immunofluorescence in a calyx terminal.

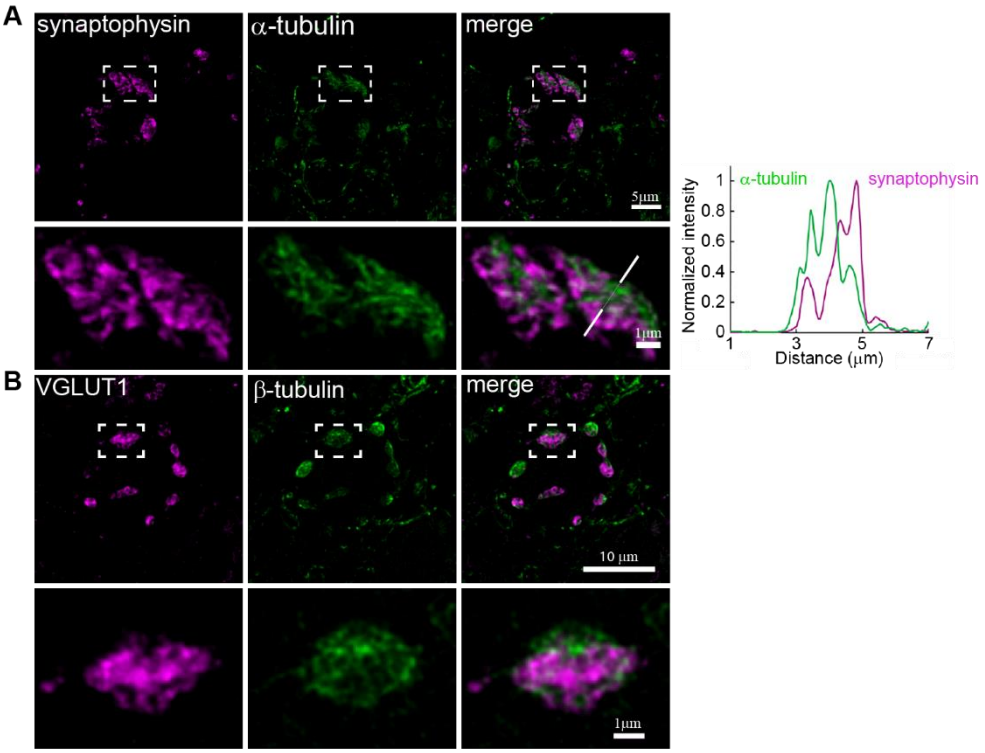

Figure 12: Co-existence of MTs in swellings of the calyx of Held presynaptic terminal

A. Example 1 of STED images of synaptophysin (magenta) and α-tubulin (green) immunofluorescence and their merged picture within a swelling of a calyceal terminal at a low magnification (upper panels). The dashed square regions are magnified in lower panels. Right graph: line-scan profile of fluorescence signal showing overlapping distributions of α-tubulin and synaptophysin immunofluorescence (along the white line in the left picture).

B. Example 2 of STED images of VGLUT1 (magenta) and β-tubulin (green) immunofluorescence within a swelling. Bottom panels illustrate high-magnification pictures taken from the dashed square areas indicated in the upper panel.

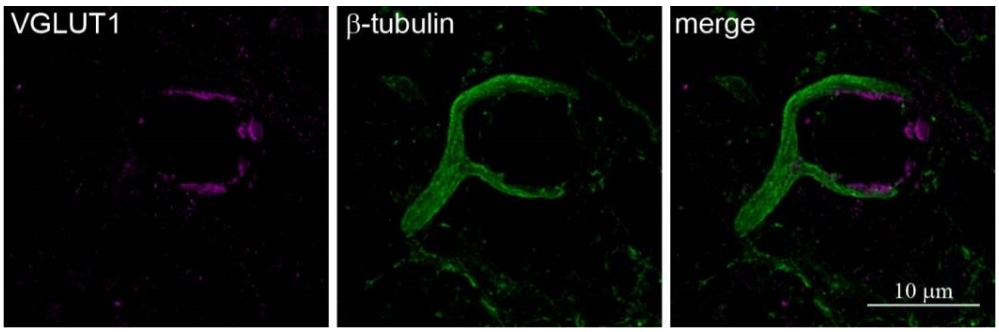

Figure 13: Distribution of MTs along fingers of calyx of Held presynaptic terminal

STED images of VGLUT1 (magenta) and β-tubulin (green) immunofluorescence along finger-like structure of a calyceal terminal.

A

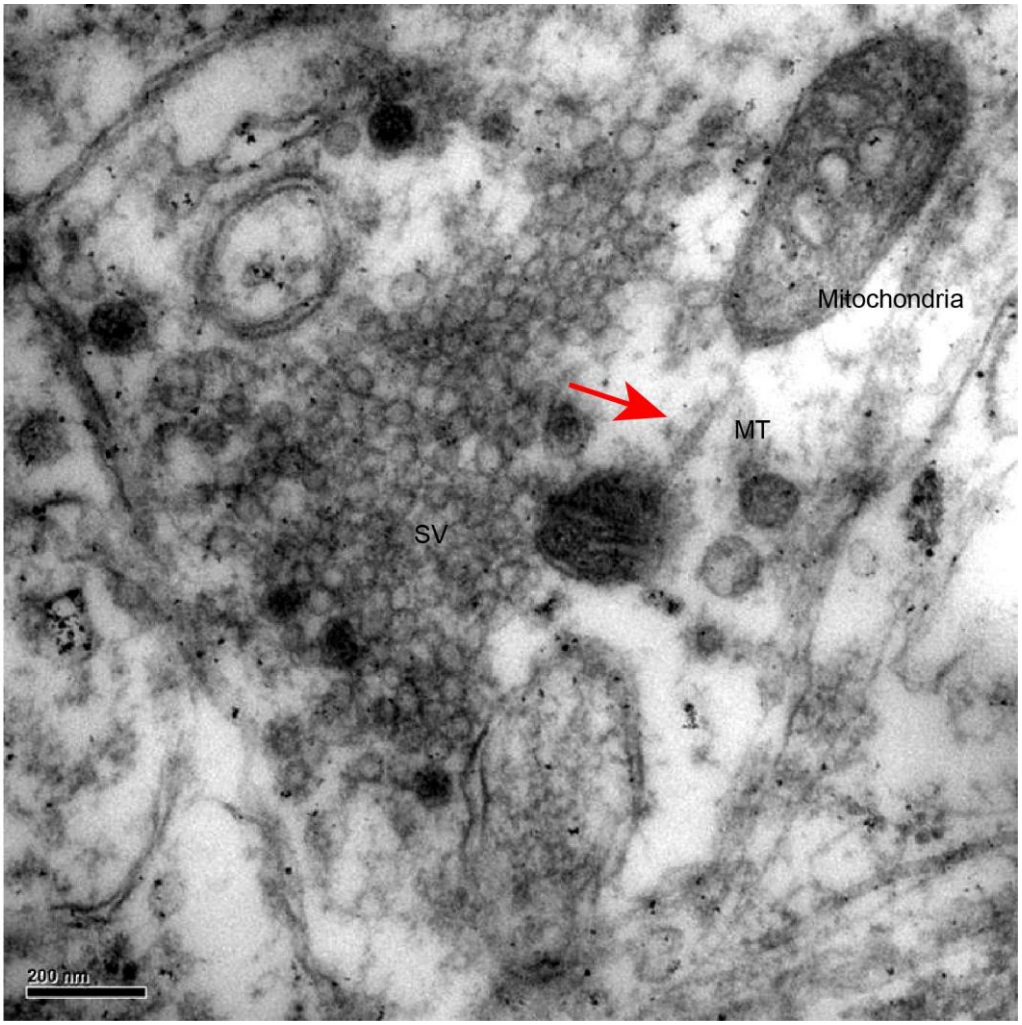

B

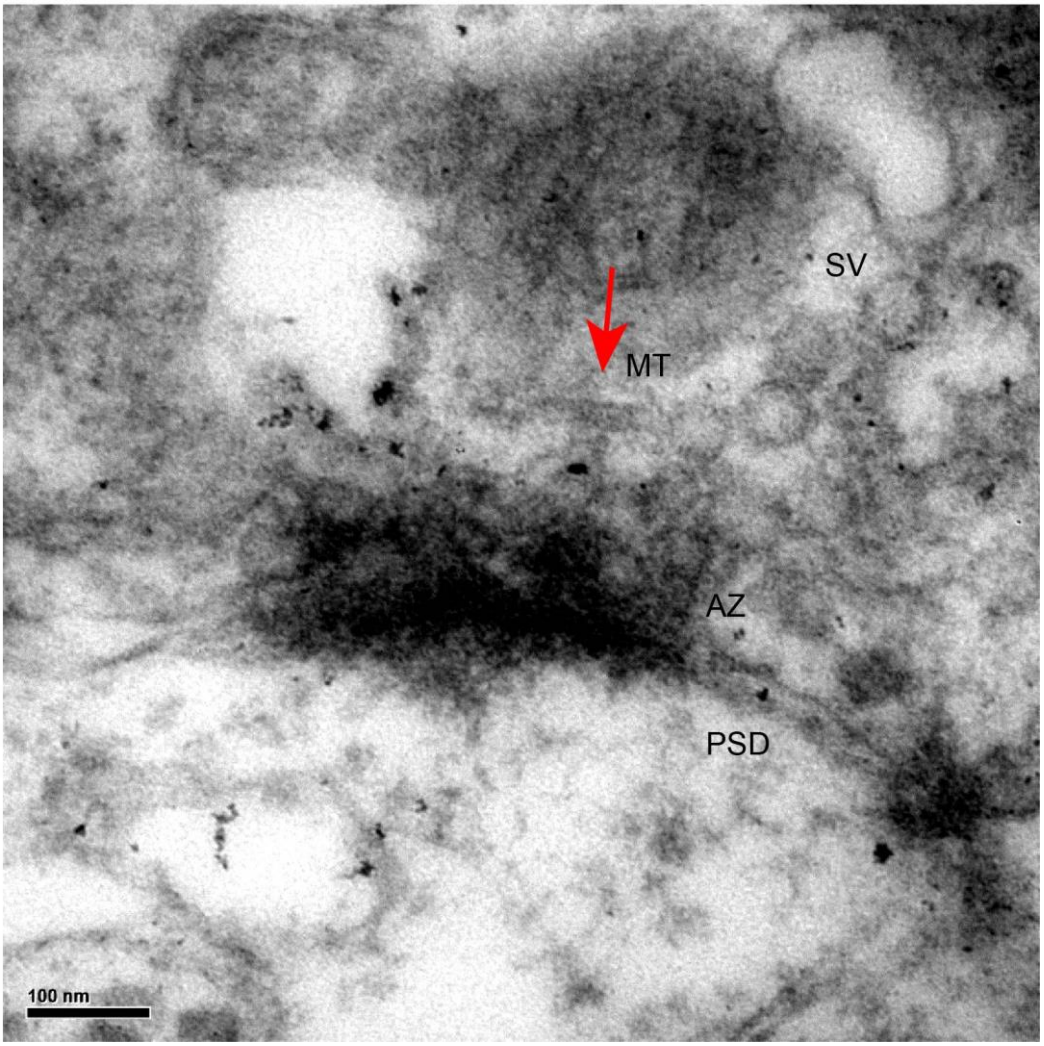

Figure 14: Electron micrographs of the calyx of Held presynaptic terminal in post-hearing rats

A. Sample EM image showing MT, SVs and mitochondria (Scale - 200 nm).

B. Sample EM image showing MT adjacent to AZ and SVs (Scale - 100 nm)

3.4 Disruption of microtubules by depolymerizing agents in acute brainstem slices from P13 rats

To address functional roles of MTs in calyceal terminals, we partially disrupted MTs using the MT depolymerizer, vinblastine. To assay the extent of MTs disrupted by vinblastine, we made a real-time imaging of presynaptic MTs in slices, using the fluorescence probe, SiR-tubulin (Lukinavicius et al., 2014; Guillaud et al., 2017), and monitored changes of MTs after vinblastine treatment. After applying SiR-tubulin in bath solution (37^{o}C), we identified calyceal terminals forming MT clusters with SiR-tubulin fluorescence (Figure 9C, Figure 15A). After bath-application of vinblastine (50 µM), fluorescently-labeled MTs were disrupted in a progressive manner, as observed from a gradual decrease in SiR-tubulin fluorescence intensity with time after drug application (Figure 9B, Figure 15B). A steep decline in SiR-tubulin fluorescence was observed in the presence of vinblastine, whereas it remained unchanged at least for 120 min in its absence. We also tested the specificity of vinblastine in depolymerizing MTs (Figure 9B, C). In the absence of vinblastine, SiR-tubulin fluorescence remained unchanged at least for 120 min (Figure 15B). SiR-tubulin fluorescence intensity declined by 50-60 % after 30-60 min incubation of slices with vinblastine (50 µM).

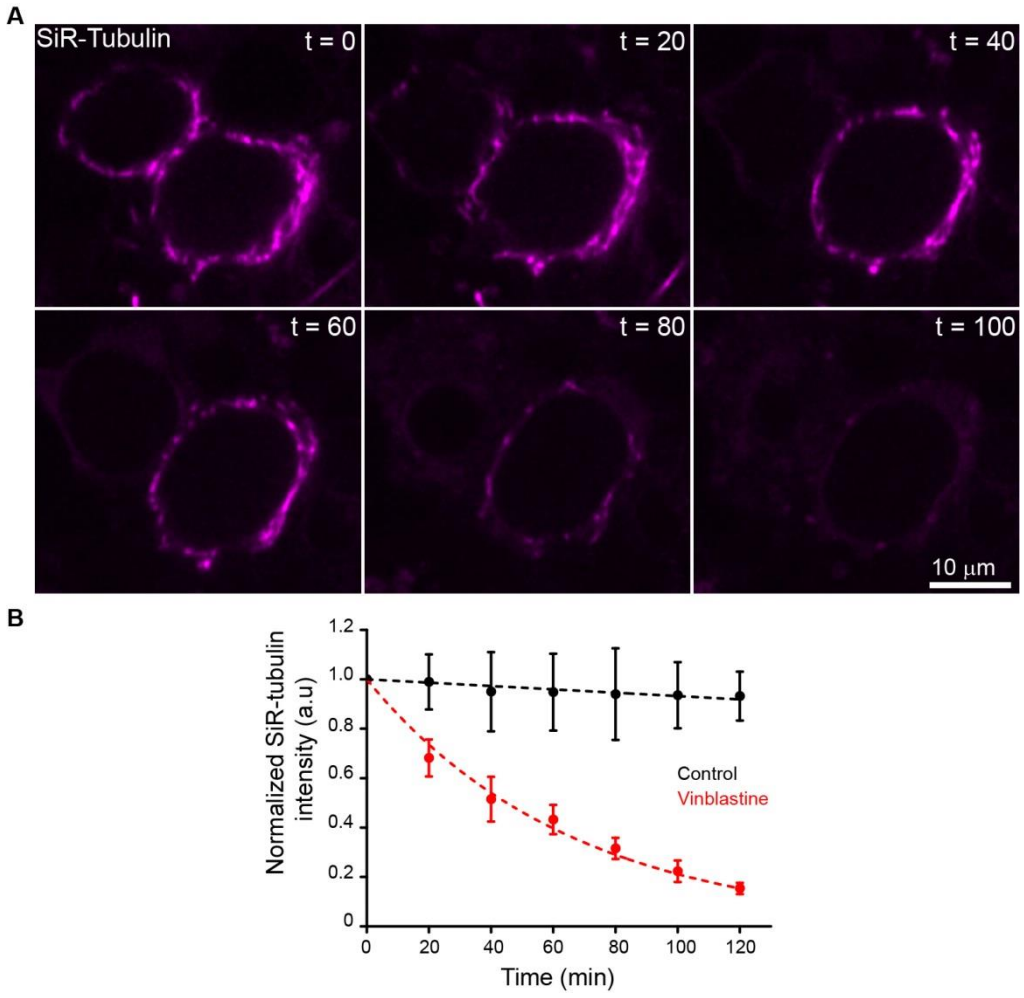

Figure 15: Progressive disruption of MTs by vinblastine treatment

A. Live staining of MTs with SiR-tubulin in slices. Sample images show the maximum projection of SiR-tubulin fluorescence in adjacent calyceal terminals, before (t = 0) and during (t = 20 to 100 min) vinblastine treatment (50 µM).

B. Time plots show progressive decrease in SiR-tubulin fluorescence intensity with time with (red) and without (black; images not shown here) vinblastine treatment (50 µM).

To ensure the effect of vinblastine treatment, using immunostaining, I quantified the fluorescence intensity of α- and β-tubulin i.r.s in paraformaldehyde-fixed brainstem slices after vinblastine treatment (Figure 16A). When slices were imaged after 60 min incubation with vinblastine (50 μM) at PT, α- and β-tubulin i.r.s declined by 40% and 50%, respectively, whereas VGLUT1 i.r.s remained unchanged (Figure 16B, *$p<0.05$). At lower concentrations (1-10 μM), vinblastine showed a concentration-dependent decline of tubulin i.r.s (Figure 16C).

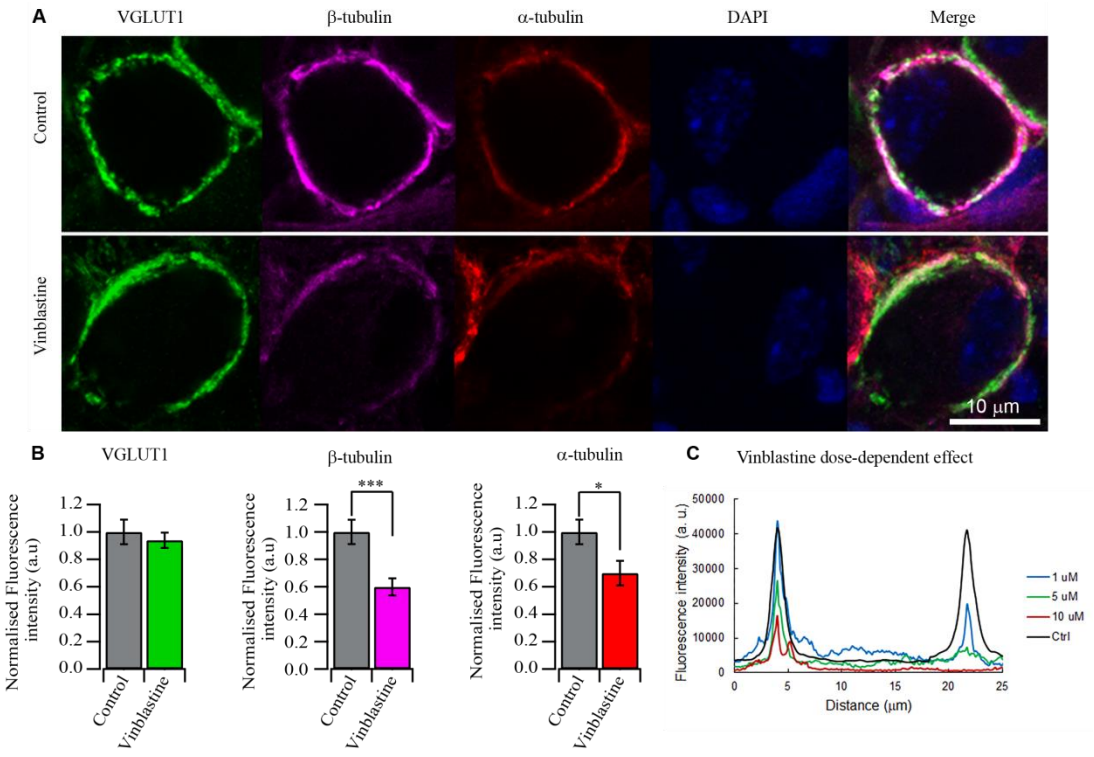

Figure 16: Vinblastine treatment affects both α- and β- tubulin isoforms in post-hearing calyx terminals

A. High-magnification confocal images of VGLUT1 (green), β-tubulin (magenta), α-tubulin (red), DAPI (blue) fluorescence without (top panel) and or with vinblastine (bottom panel; t = 60 mins) at PT.

B. Bar graphs indicate reductions of VGLUT1 (left; control n = 31; vinblastine n = 28; from 3 slices of 3 animals), β-tubulin (middle; control n = 20; vinblastine n = 23), α-tubulin (right; control n = 20; vinblastine n = 23) immunofluorescence signal intensity 60 min after vinblastine treatment (50 µM). *p<0.05.

C. Summary plot indicating asymmetrical reduction in α- and β-tubulin i.r.s after treatment with different concentrations of vinblastine (1 µM - blue, 5 µM - greens, 10 µM - red) compared to control (black).

3.5 Vinblastine desynchronizes nerve-evoked quantal release and increases spontaneous quantal release

I next examined whether partial MT disruption by vinblastine treatment affects basal synaptic transmission in post-hearing rat calyceal synapses. Vinblastine treatment for ~60 min had no effect on the amplitude of EPSCs, but significantly prolonged their rise and decay times (Figure 17A, B). In contrast, vinblastine treatment had no effect on rise time or decay time or amplitude of mEPSCs (Figure 18A, B). However, like latrunculin A (Figure 7), vinblastine treatment markedly increased mEPSC frequency (Figure 18A, B). A prolonged decay time of evoked EPSCs, unassociated with that of mEPSCs, suggests a decrease in the rate of quantal release. To measure the magnitude of desynchronization, I performed the deconvolution analysis to estimate the release rate of SVs (Neher and Sakaba, 2001; Sakaba and Neher, 2001b). After vinblastine treatment, duration of quantal release in response to an AP was significantly prolonged, with half-maximal duration becoming from 0.23 ms (0.231 ± 0.0086, n = 5) to 0.27 ms (0.275 ± 0.0077, n = 6, p = 0.0039; Figure 19 A, B). These results indicate that partial disruption of MTs desynchronizes quantal transmitter release, implicating that MTs might be involved in positional priming of SVs.

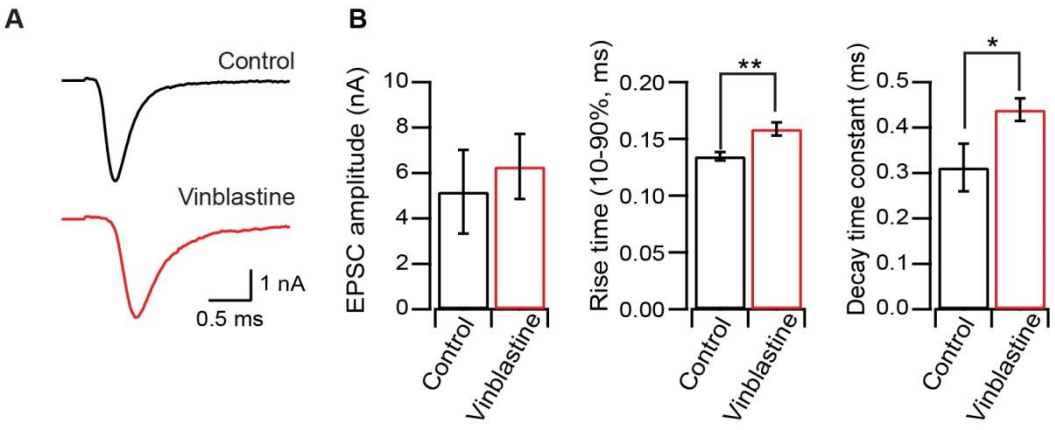

Figure 17: MT disruption prolongs EPSC kinetics in post-hearing rats

A. Sample traces of EPSCs with (red) and without (black) vinblastine treatment recorded at PT.
B. Bar graphs compare EPSCs between control (n = 5) and vinblastine treatment (n = 6) with respect to mean amplitude (no difference, p = 0.639), rise time (10-90%, significant difference, p = 0.008) and decay time constant (significant difference, p = 0.044). Kyn (2 mM) was included in aCSF to minimize saturation and desensitization of postsynaptic receptors.

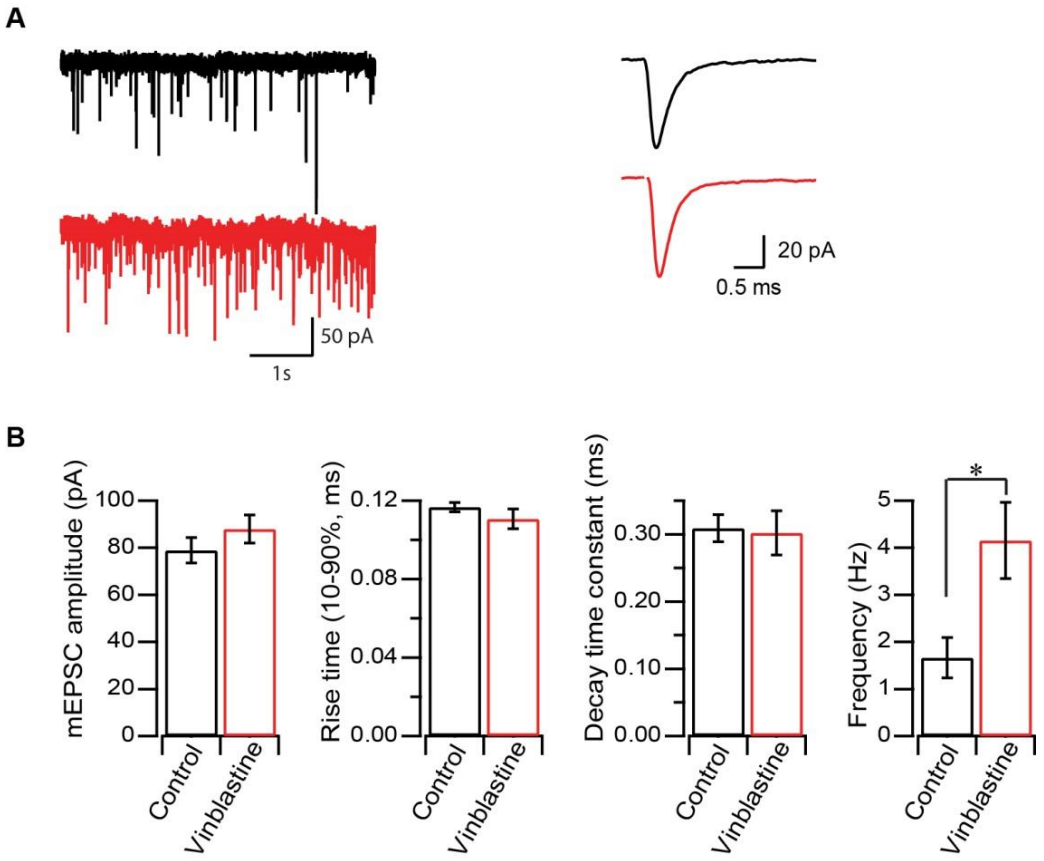

Figure 18: MT disruption increases spontaneous quantal release

A. Sample mEPSC records with (red) and without (black) vinblastine treatment at a slow sweep speed (left) and single mEPSC at a faster sweep (right) recorded at PT.

B. Bar graphs compare mEPSCs between control (n = 9) and vinblastine treatment (n = 9) with respect to mean amplitudes (no difference, p = 0.279), rise time (10-90) % (no difference, p = 0.278), decay time constant (no difference, p = 0.862) and frequencies of mEPSCs (significant difference, p = 0.015) with and without vinblastine treatment. ACSF contained no kyn acid in these experiments.

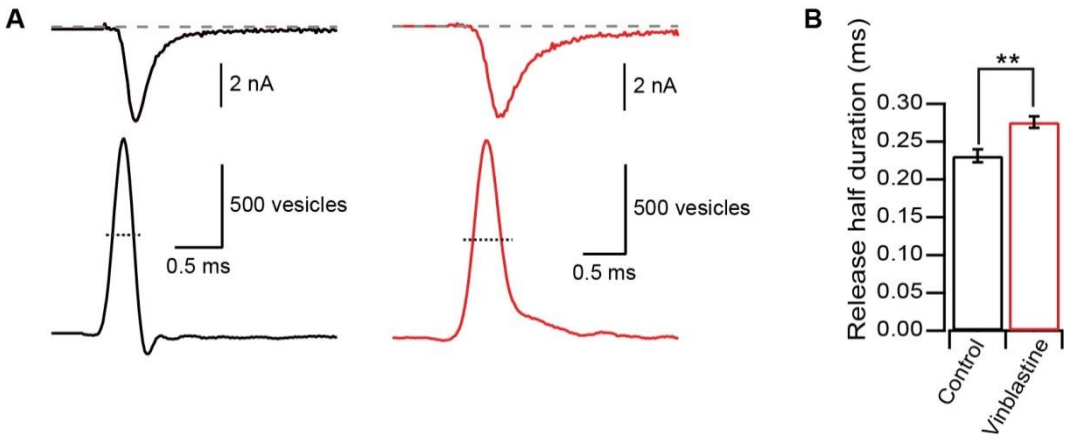

Figure 19: Vinblastine desynchronizes nerve-evoked quantal release

A. Sample EPSCs (upper traces) and release rates (lower traces) with (red) or without (black) vinblastine treatment at PT.
B. Bar graphs compare half maximal duration of release rates between control and vinblastine treatment Significant difference with $p = 0.003$ (control $n = 5$; vinblastine $n = 6$).

3.6 Effect of MT disruption on dynamic synaptic functions

Synaptic transmission is maintained by rapid recycling of SVs in the presynaptic terminal. Since MTs are involved in long-distance trafficking of SVs in cultured calyceal presynaptic terminals (Guillaud et al., 2017), I examined whether they might be involved in the recovery of EPSCs from STD. After 100 Hz x 30 train stimulation, EPSCs underwent an STD (Figure 20A). The quantal parameters Nq and Pr estimated from cumulative EPSCs did not change after vinblastine treatment (Figure 21B). After STD, EPSCs recovered within 10 s to initial level with a bi-exponential time course (Figure 22 A, B). The weighted mean time constant of the recovery (see Materials and Methods) was 0.62 ± 0.09 s (Figure 22A) that is much faster than that at RT (1.72 ± 0.32, Figure 6) for calyces of post-hearing rats. When we treated slices with vinblastine (50 µM for 30-60 min) to disrupt MTs by 50-60% (Figure 15), the slow recovery time constant (τ_s) became significantly slower ($p = 0.031$, $n = 10$), whereas the fast time constant (τ_f) remained unchanged ($p = 0.59$, Figure 22B). The weighted mean recovery time constants (τ_m) was significantly slowed ($p = 0.005$). There was a positive correlation ($R = 0.892$) between the weighted mean recovery time constants (τ_m) and the magnitude of MT disruption (Figure 22C). These results were essentially the same when STD was induced by a train of 300 Hz stimulation instead of 100 Hz stimulation (Figure 23A, B).

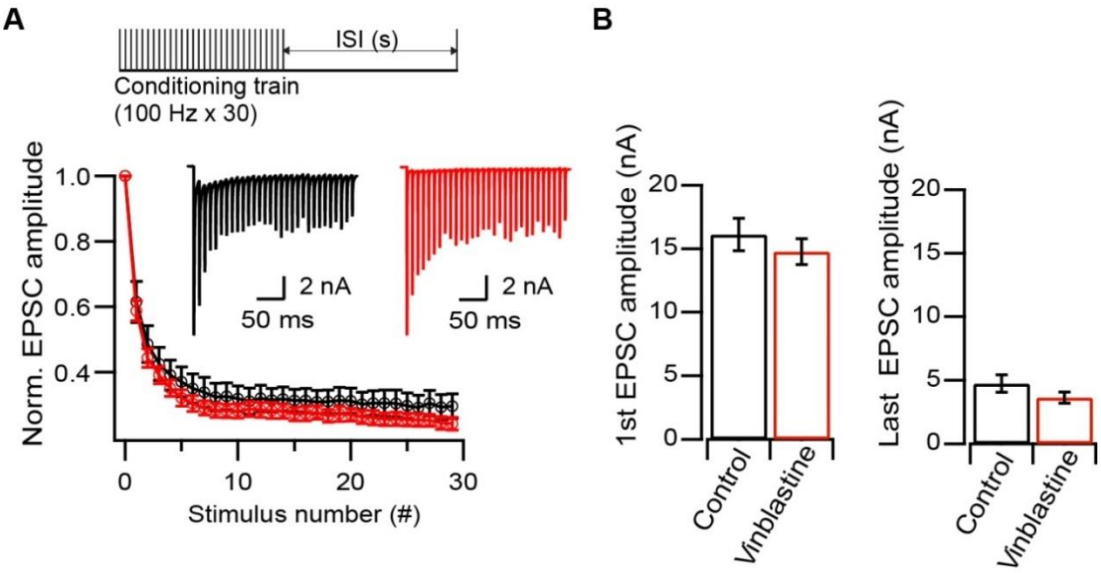

Figure 20: Effect of MT disruption on steady state EPSC amplitude

A. *Upper panel.* Stimulation protocol for inducing STD and recovery; 30 stimulation pulses at 100 Hz followed by a test pulse at different intervals (0.02-10s).

   Middle panel. Sample traces of EPSCs undergoing STD with (red) or without (black) vinblastine treatment at PT.

   Lower panel. EPSC amplitudes during a train of 30 stimuli at 100 Hz in control (black; n = 6) and vinblastine (red; n = 10) at PT.

B. Bar graphs summarize the comparison between initial (left) and last (right) EPSC amplitude with (red) or without (black) vinblastine treatment.

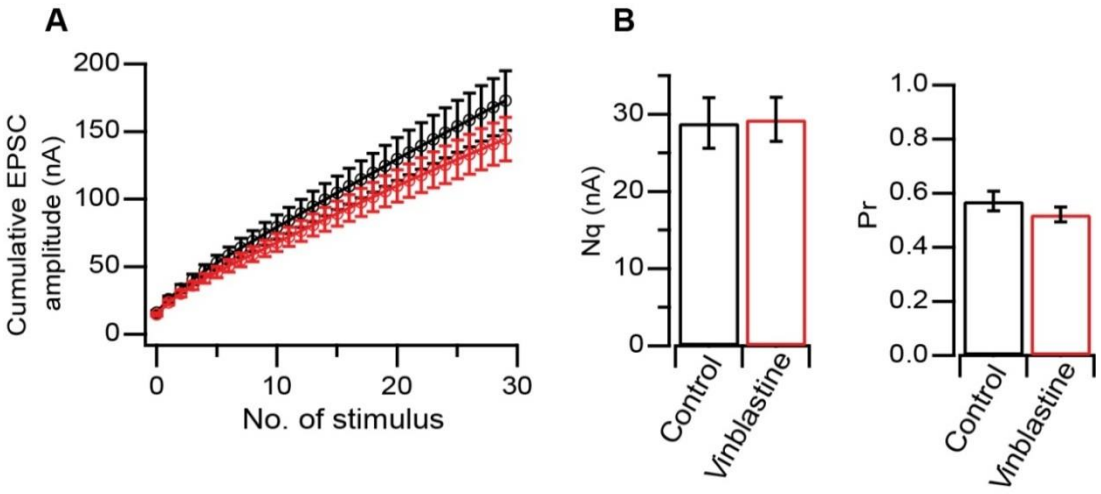

Figure 21: MT disruption has no effect on RRP size or release probability in post-hearing rats

A. Cumulative EPSC amplitudes during the train of stimulation with (red) or without (black) vinblastine treatment.

B. Bar graphs summarize the comparison between the RRP size (Nq) and release probability (Pr) between synapses with (red) or without (black) vinblastine treatment.

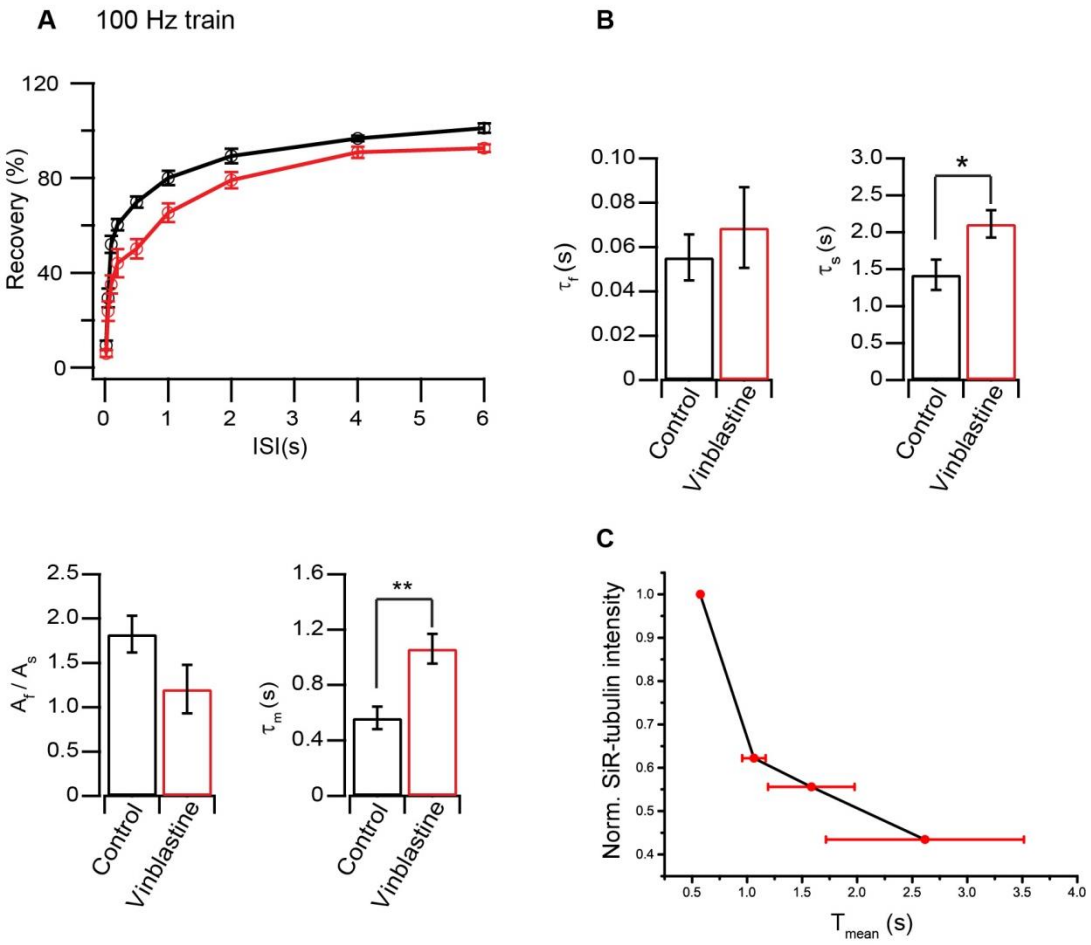

Figure 22: MT disruption slows the recovery of EPSCs from STD after 100 Hz train

A. Recovery time course of EPSCs with (red) or without (black) vinblastine treatment after 100 Hz train recorded at PT.

B. Bar graphs indicate fast recovery time constant (τ_f), slow time constant (τ_s), their relative proportion (A_f / A_s) and weighted mean time constant ($[(A_f\tau_f + A_s\tau_s)]$). *$p < 0.05$ in Student t-test, control n = 6; vinblastine n = 10.

C. Correlation between normalized SiR-tubulin intensity and weighted mean recovery time constant of EPSCs from STD after different length of vinblastine treatment (30-120 min) at PT.

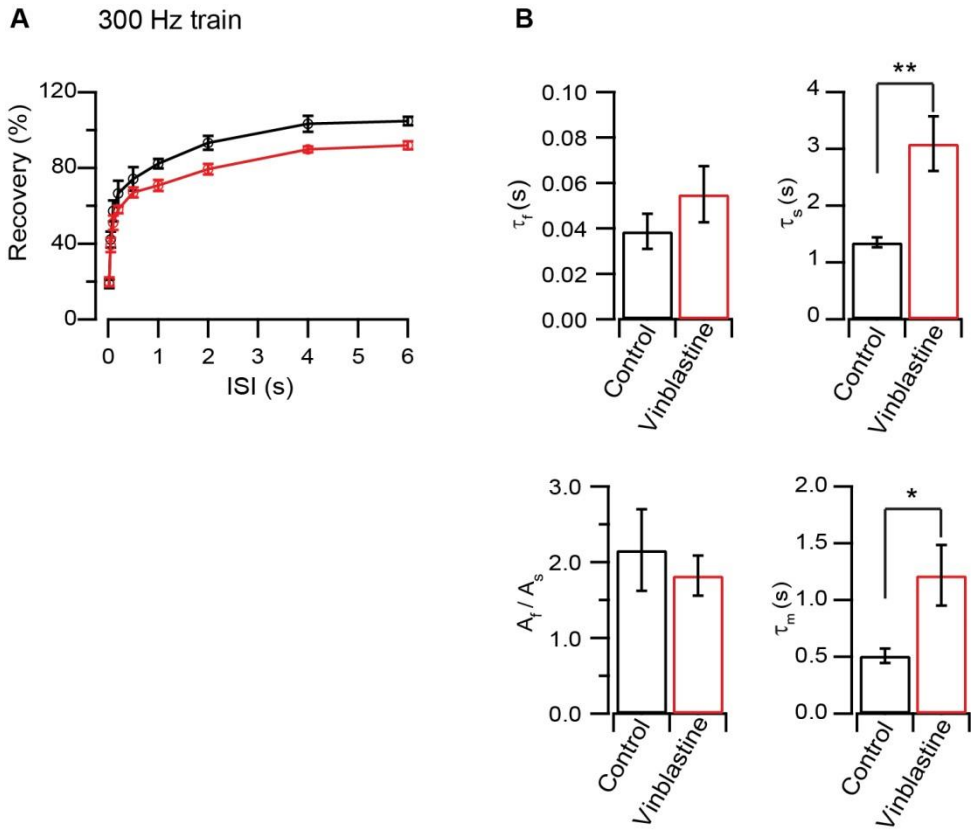

Figure 23: MT disruption also slows the recovery of EPSCs from STD after 300 Hz train

A. Recovery time course of EPSCs with (red) or without (black) vinblastine treatment after 300 Hz train of stimulation at PT.

B. Bar graphs indicate fast recovery time constant (τ_f), slow time constant (τ_s), their relative proportion (A_f / A_s) and weighted mean time constant ($[(A_f\tau_f + A_s\tau_s)]$) with (n = 8) or without (n = 6) vinblastine treatment. *p < 0.05 in Student t-test.

3.7 MT disruption by vinblastine has no effect on vesicle exo-endocytosis or presynaptic Ca^{2+}currents

The slow component of recovery time from STD often runs parallel with the time course of vesicle endocytosis after various drug treatments and therefore proposed to reflect the time of SV endocytosis (Hosoi et al., 2007). We tested whether MT disruption by vinblastine affects vesicle endocytosis, using membrane capacitance measurements from calyceal terminals (Sun et al., 2002; Yamashita et al., 2005) at PT. Exo-endocytic changes of membrane capacitance were triggered by presynaptic Ca^{2+} currents elicited by a 20 ms pulse stepping from -80 mV to 10 mV. Vinblastine treatment (50 µM, 30-60 min) had no effect on endocytic time course, exocytic magnitude (ΔC_m), or presynaptic Ca^{2+} current charge (Q_{Ca}; Figure 24A, B). These results suggest that MT disruption has no effect on SV exocytosis or endocytosis in calyceal terminals indicating that recovery time from STD is not a simple reflection of SV endocytic time alone, but contains time for SV transport to release sites that depends in part on MTs.

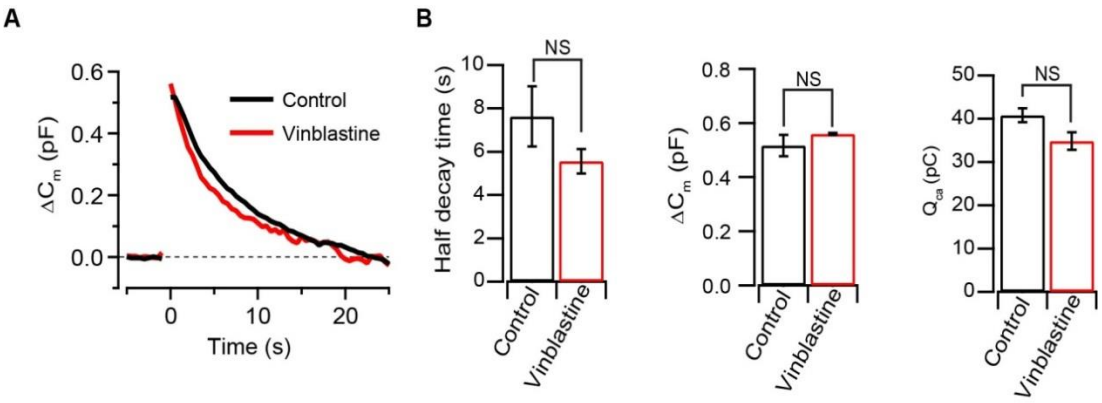

Figure 24: No effect of MT disruption on exo-endocytosis at calyces of Held terminals

A. Vinblastine treatment had no effect on the magnitude of exocytosis (ΔC_m) or endocytic time course. Averaged traces of ΔC_m recorded from with (n = 5 terminals, red) or without (n = 4, black) vinblastine treatment (superimposed) recorded at PT.

B. Bar graphs summarizing endocytic half decay time (left), exocytic magnitude (ΔC_m, right) and Ca^{2+} current charge (Q_{ca}) with (red) or without (black) vinblastine treatment (50µM, 30-60 min).

Importance of microtubule network for synaptic vesicle trafficking in cultured calyces

Mechanisms underlying exo-endocytosis have been extensively studied, but little is known for the mechanism that operates between endocytosis and exocytosis to deliver SVs to release sites. Some presynaptic terminals rapidly reuse SVs after endocytosis (Rea et al., 2004) whereas vesicles are kept for long in a reserve pool at other terminals (Hilfiker et al., 1999). Molecular mechanisms regulating SV mobility remains open.

In hippocampal synaptic boutons in culture, actin disruption reportedly upregulates (Jordan et al., 2005), or downregulates (Lee et al., 2012b) mobility of SVs. Actin disruption inhibits long SV trafficking that spans across cultured hippocampal synaptic boutons (Darcy et al., 2006), whereas MT disruption by nocodazole inhibits long SV trafficking in calyceal terminals in culture (Guillaud et al., 2017). I reinvestigated the latter issue using vinblastine in calyceal terminals in culture (Dimitrov et al., 2016) by labeling SVs using quantum dots (Guillaud et al., 2017).

3.8 MTs are involved in long-distance trafficking of SV

Three decades ago, Gray found that MTs attached with SVs extend to AZs of motor nerve terminals (Gray, 1983), thereby postulated that MTs may translocate SVs to release sites. However, later studies did not support his proposal, making functional roles of MTs regulating SV mobility elusive.

At calyceal terminals in culture, MT-based SV movements have been shown by real-time imaging of SVs using quantum dots (Guillaud et al., 2017). I revisited this issue using vinblastine (10 µM) instead of nocodazole (Guillaud et al., 2017). Fluorescence intensity of SiR-tubulin stained calyceal terminals decreased by ~50% after 90 min incubation with 10µM vinblastine (Figure 25A-C) like nocodazole (30 µM, Figure 25C). The distribution of trajectories estimated by Imaris software showed that MT disruption reduced the proportion of SVs traveling along long directional trajectories (> 4 µm; Guillaud et al., 2017) by 48 %, with little effect on shorter trajectories (< 2 µm, Figure 26A, B). These results confirm that MT depolymerization reduces the proportion of SVs traveling long distances at the giant calyceal terminal in culture (Guillaud et al., 2017).

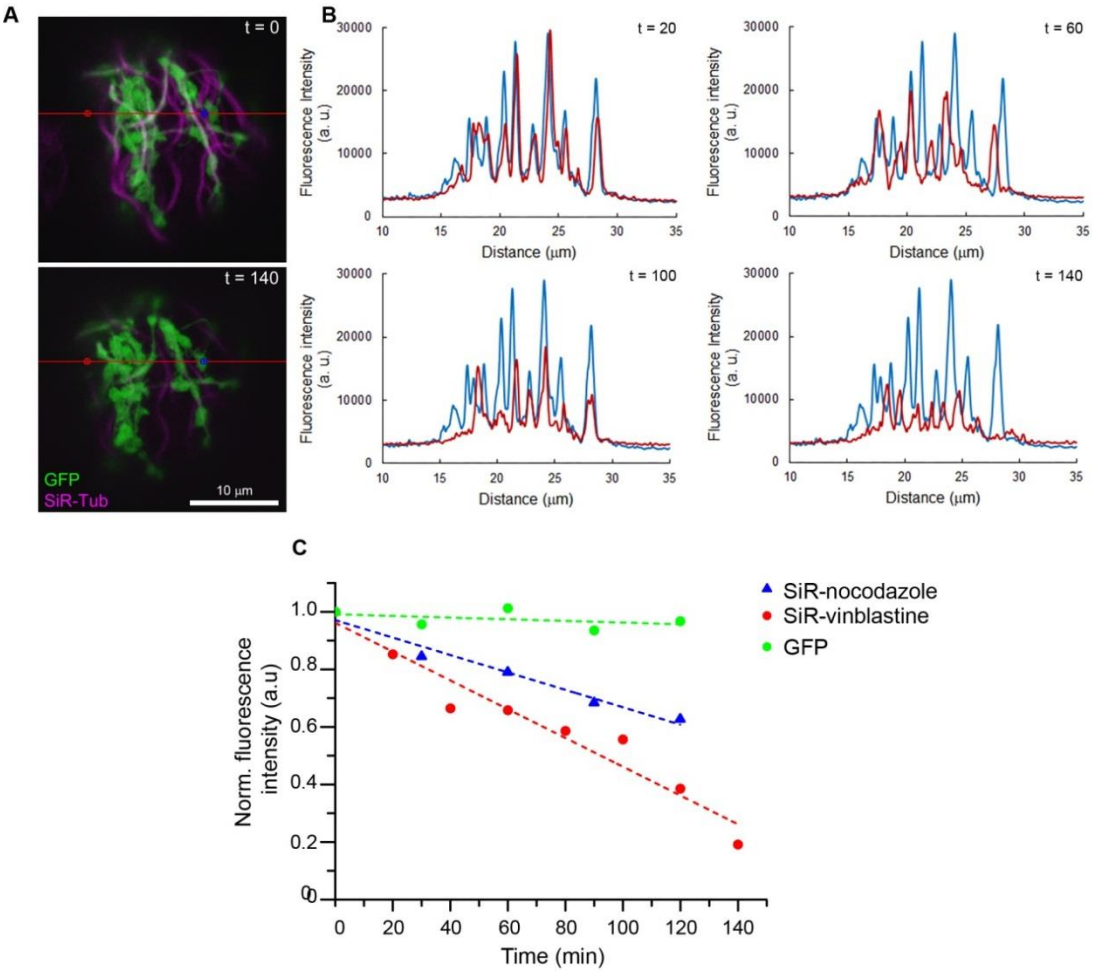

Figure 25: MTs are disrupted in a time-dependent manner

A. Live confocal imaging of calyceal terminal over-expressing GFP and labelled with SiR-tubulin before (top; t = 0 min) and after (bottom; t = 140 min) vinblastine (10 µM) treatment.
B. Fluorescence intensity line profiles of calyceal terminals during treatment (0-140 min) with (red) or without vinblastine (blue).
C. Summary graph comparing the SiR-tubulin fluorescence intensity in GFP (control), during nocodazole treatment (30 µM), and during vinblastine treatment (10 µM).

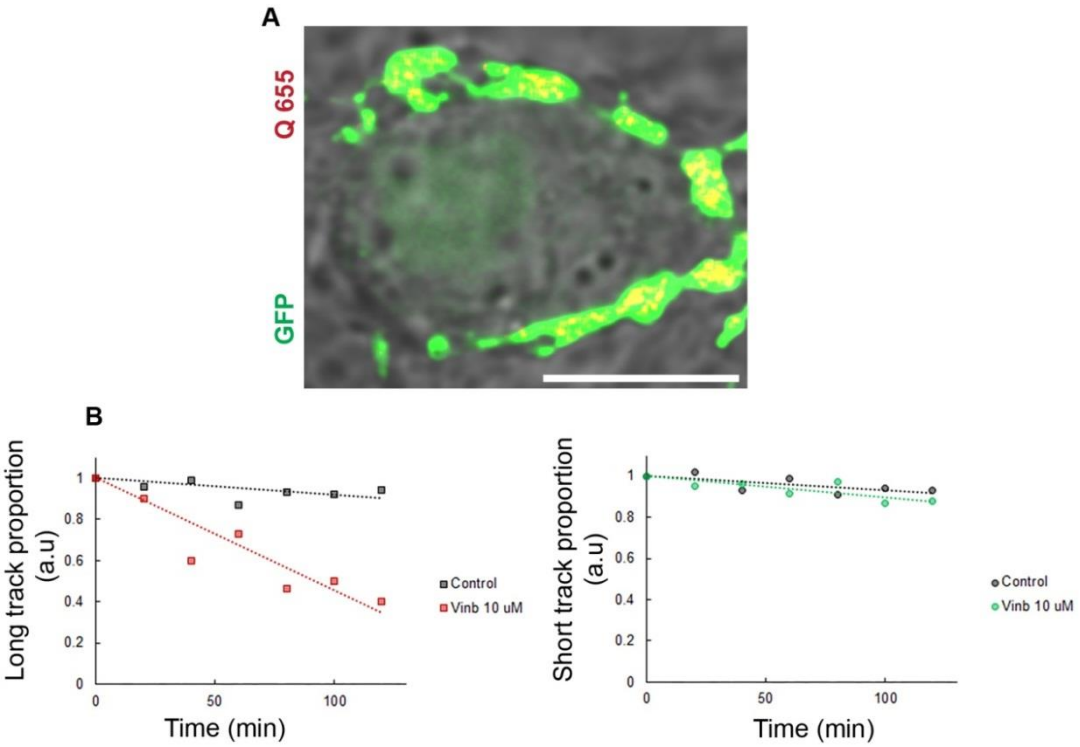

Figure 26: Presynaptic MTs regulates long distance SV movements

A. Live confocal imaging of a calyceal terminal expressing cytosolic GFP and Q655-syt2 labelled SVs. Scale - 10µm.
B. Summary graphs comparing the proportion of vesicles moving along long (> 4 µm, left, red) and short (< 2 µm, right, green) tracks within 30 s observation period with or without (grey) vinblastine (10 µM) treatment.

4. DISCUSSION

Among cytoskeletal proteins in the nerve terminals, there is accumulating evidence for the roles of actin in neurotransmission. In contrast, little is known for the functional role of MTs in presynaptic terminals. In the present study, at the calyx of Held in slices of juvenile rats, I found that partial disruption of MTs with vinblastine can desynchronize quantal transmitter release and impair the recovery of neurotransmission from STD. These results suggest that MTs play roles for fast transmitter release as well as for efficient retrieval of SVs to maintain neurotransmission.

Roles of actin filament in nerve terminals

I reproduced a previous report (Sakaba and Neher, 2003) that F-actin disruption by latrunculin A slows the recovery of EPSCs from STD at P7-P9 rats before the hearing onset. However, in post-hearing rats (P13-P15), I found that latrunculin A no longer affected the recovery of EPSCs from STD. These results suggest that the involvement of actin filaments in SV recycling is a developmental phenomenon at the calyx of Held.

At the rodent calyx of Held, developmental changes are often observed for many presynaptic mechanisms, particularly before and after hearing onset. To cite a few, GTP-independent component of endocytosis becomes negligible after hearing (Yamashita et al., 2010), presynaptic Ca^{2+} channel subtypes switches from mixed N, P/Q, R types to predominantly P/Q type (Iwasaki and Takahashi, 1998; Iwasaki et al., 2000). Presynaptic regulatory molecular mechanisms downstream of Ca^{2+} influx, such as calmodulin-dependent inactivation of Ca^{2+} channels (Xu and Wu, 2005), or calcineurin-dependent endocytosis (Yamashita et al., 2010) becomes non-functional after hearing (Nakamura et al., 2008), likely due to a developmental reduction in the size of Ca^{2+} nanodomain (Yamashita et al., 2010) associated with shortening in the Ca^{2+}-release coupling distance (Nakamura et al., 2015). Since MLCK-actin-dependent slowing mechanism of recovery from STD resides downstream of calmodulin (Sakaba and Neher, 2003), lack of effect of latrunculin A on the

recovery from STD after hearing in the present study (Figure 6) may be caused by a developmental reduction in the contribution of calmodulin to presynaptic regulation.

Latrunculin A treatment slowed the decay time of EPSCs at calyces of Held in slices from both pre- and post-hearing rats. Furthermore, it increased mEPSC frequency by several times in post-hearing rat calyces with no significant effect on its decay time. These results are consistent with the suggestion that F-actin anchors SVs for positional-priming (Lee et al., 2012a). Latrunculin A might then untether SVs, thereby slowing the EPSC decay time and increasing spontaneously releasing SVs.

Microtubules in the presynaptic terminal

Although somewhat controversial in the past reports (Gray, 1975; Perkins et al., 2010), I found MTs in the calyx of Held, often co-localized with SVs when observed using STED microscopy. I then made partial disruption of MTs using vinblastine, which prevents tubulin polymerization and disintegrates MT filaments (Jordan et al., 1992). I confirmed that its effect was specific on MTs with no effect on actin filaments. In most previous studies, genetic ablation or pharmacological disruption of cytoskeletal proteins have been made without estimating their effects on cytoskeletal filaments. Massive destruction of cytoskeletal elements can destroy cell structures and may cause secondary effects thereby. To estimate the effect of vinblastine disrupting MTs, I monitored its effect on MTs both in real time using SiR-tubulin and after fixation using immunofluorescence staining. Both results provided a condition, in which MTs in calyces are disrupted by ~50%.

Disruption of calyceal MTs by ~50 % slowed rise time and decay time kinetics of EPSCs recorded at PT. Like after actin filament disruption, MT disruption markedly increased mEPSC frequency without affecting their rise or decay times. These results suggest that slowing of EPSCs by vinblastine is caused by its effect on presynaptic MTs. Deconvolution analysis indicated that MT disruption slows the rate of quantal release. These results when taken together with those after actin disruption suggest that both actin and MT filaments could

contribute to tethering and positional priming of SVs at the calyx of Held and that their disruption increases the asynchronous release of SVs from presynaptic terminals.

In the STD protocol at PT, I found that partial disruption of MTs by vinblastine slowed the recovery of EPSCs from STD. This effect was specific for the slow recovery component with no effect on the fast recovery component. Although the slow recovery component is implicated for the endocytic time of SV retrieval (Hosoi et al., 2007), capacitance measurements revealed no change in endocytic time course or exocytic magnitude after vinblastine treatment. These results suggest that the slow recovery from STD is not a simple reflection of SV endocytic time, but it also contains the time for SV transport to the release sites and that this SV replenishment is mediated, at least in part, by MTs.

MT disruption had no effect on the fast recovery from STD, which however is attenuated by pharmacological disruption of actin filaments or its regulatory molecular cascades involving MLCK (Ryan, 1999; Sakaba and Neher, 2003; Jordan et al., 2005) and RIM (Schoch et al., 2002) at pre-hearing rat calyces. It seems that immediate SV replenishment after RRP depletion relies on actin filaments (Lee et al., 2012a), whereas slow replenishment of recycling SVs is mediated by long SV traffic along MTs, thereby maintaining high-frequency neurotransmission for a sustained period of time.

MTs are known to carry mitochondria toward AZ to fuel SV retrieval and recycling (Perkins et al., 2010) as well as to take up excess Ca^{2+} (Tang and Zucker, 1997; Jonas et al., 1999) in presynaptic terminal cytosols. Therefore, it is possible that the slowed recovery from STD by vinblastine might be a secondary effect of mitochondrial arrest. From the present results, this possibility cannot be excluded.

Nevertheless, an attractive hypothesis for the role of presynaptic MTs is SV transport to release sites (illustration 3). In cultured calyceal synapses, movements of SVs along long tracks is selectively blocked by treatment with MT depolymerizers, nocodazole (Guillaud et al., 2017) or vinblastine (this study). As there is no

evidence to support that the MT-mediated long track SV movements are directed toward release sites, this would be an important issue to be investigated. Also, it would be interesting to investigate the interplay between actin and MT filaments at the presynaptic terminal, to answer how they co-regulate synaptic transmission.

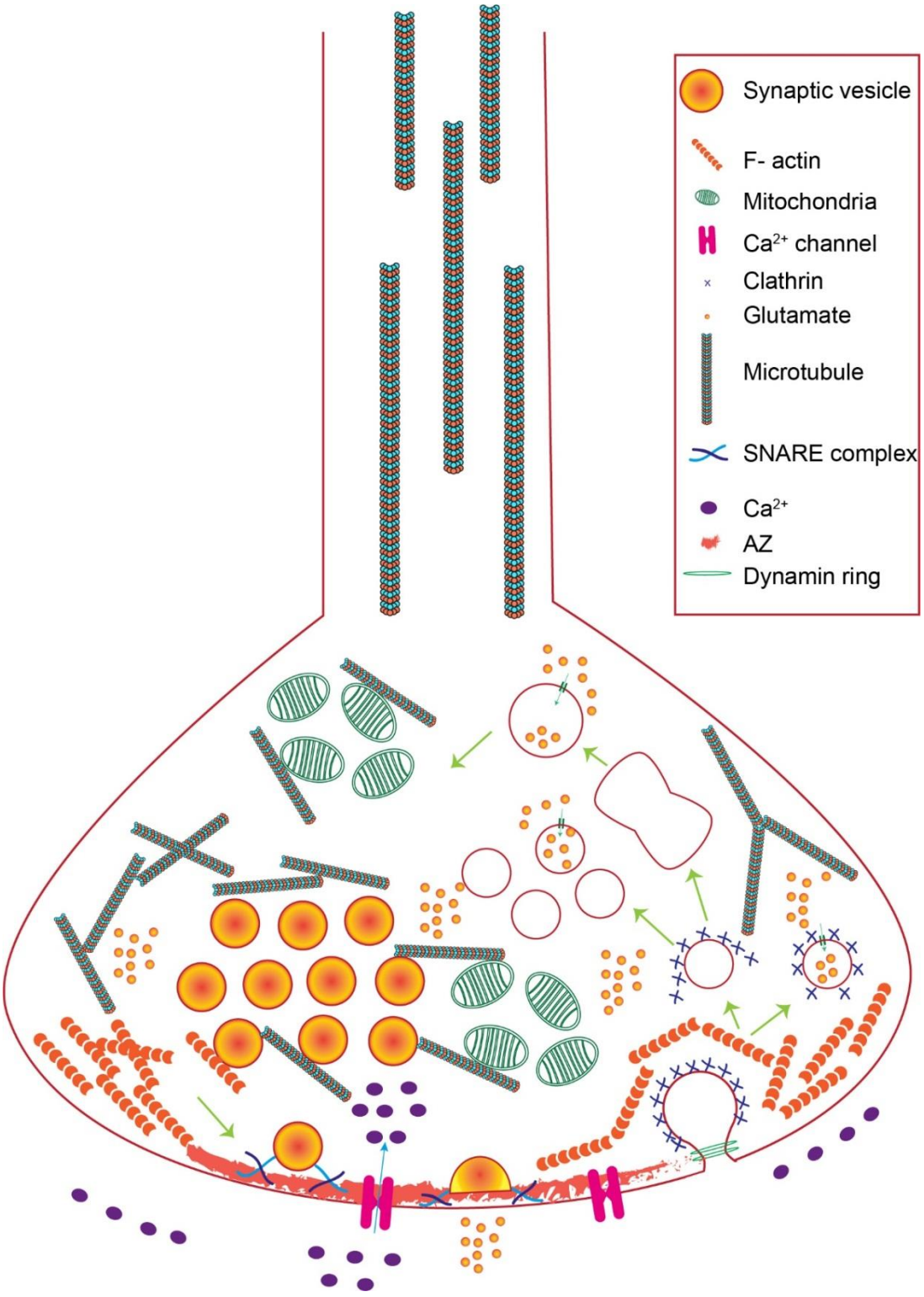

Illustration 3: Proposed modified schematic illustration of SV cycles

MTs are positioned close to mitochondria, SVs. Some are found approaching release sites in this illustration.

REFERENCES

Albrecht, O., Dondzillo, A., Mayer, F., Thompson, J.A., and Klug, A. (2014). Inhibitory projections from the ventral nucleus of the trapezoid body to the medial nucleus of the trapezoid body in the mouse. Front Neural Circuits *8*, 83.

Allison, D.W., Gelfand, V.I., Spector, I., and Craig, A.M. (1998). Role of actin in anchoring postsynaptic receptors in cultured hippocampal neurons: differential attachment of NMDA versus AMPA receptors. J Neurosci *18*, 2423-2436.

Amilhon, B., Lepicard, E., Renoir, T., Mongeau, R., Popa, D., Poirel, O., Miot, S., Gras, C., Gardier, A.M., Gallego, J., *et al.* (2010). VGLUT3 (vesicular glutamate transporter type 3) contribution to the regulation of serotonergic transmission and anxiety. J Neurosci *30*, 2198-2210.

Ashton, A.C., and Dolly, J.O. (1997). Microtubules and microfilaments participate in the inhibition of synaptosomal noradrenaline release by tetanus toxin. J Neurochem *68*, 649-658.

Baas, P.W., Deitch, J.S., Black, M.M., and Banker, G.A. (1988). Polarity orientation of microtubules in hippocampal neurons: uniformity in the axon and nonuniformity in the dendrite. Proc Natl Acad Sci U S A *85*, 8335-8339.

Balschun, D., Moechars, D., Callaerts-Vegh, Z., Vermaercke, B., Van Acker, N., Andries, L., and D'Hooge, R. (2010). Vesicular glutamate transporter VGLUT1 has a role in hippocampal long-term potentiation and spatial reversal learning. Cereb Cortex *20*, 684-693.

Betz, W.J., and Henkel, A.W. (1994). Okadaic acid disrupts clusters of synaptic vesicles in frog motor nerve terminals. J Cell Biol *124*, 843-854.

Billups, B. (2005). Colocalization of vesicular glutamate transporters in the rat superior olivary complex. Neurosci Lett *382*, 66-70.

Bird, M.M. (1976). Microtubule--synaptic vesicle associations in cultured rat spinal cord neurons Cell Tissue Res *168*, 101-115.

Bleckert, A., Photowala, H., and Alford, S. (2012). Dual pools of actin at presynaptic terminals. J Neurophysiol *107*, 3479-3492.

Blitz, A.L., and Fine, R.E. (1974). Muscle-like contractile proteins and tubulin in synaptosomes. Proc Natl Acad Sci U S A *71*, 4472-4476.

Bloom, O., Evergren, E., Tomilin, N., Kjaerulff, O., Low, P., Brodin, L., Pieribone, V.A., Greengard, P., and Shupliakov, O. (2003). Colocalization of synapsin and actin during synaptic vesicle recycling. J Cell Biol *161*, 737-747.

Borisy, G.G., and Taylor, E.W. (1967). The mechanism of action of colchicine. Binding of colchincine-3H to cellular protein. J Cell Biol *34*, 525-533.

Burke, B.E., and DeLorenzo, R.J. (1981). Ca^{2+}- and calmodulin-stimulated endogenous phosphorylation of neurotubulin. Proc Natl Acad Sci U S A *78*, 991-995.

Burke, B.E., and DeLorenzo, R.J. (1982). Ca^{2+} and calmodulin-dependent phosphorylation of endogenous synaptic vesicle tubulin by a vesicle-bound calmodulin kinase system. J Neurochem *38*, 1205-1218.

Carlson, M.D., Kish, P.E., and Ueda, T. (1989). Characterization of the solubilized and reconstituted ATP-dependent vesicular glutamate uptake system. J Biol Chem *264*, 7369-7376.

Ceccarelli, B., Grohovaz, F., and Hurlbut, W.P. (1979). Freeze-fracture studies of frog neuromuscular junctions during intense release of neurotransmitter. II. Effects of electrical stimulation and high potassium. J Cell Biol *81*, 178-192.

Ceccarelli, B., Hurlbut, W.P., and Mauro, A. (1973). Turnover of transmitter and synaptic vesicles at the frog neuromuscular junction. J Cell Biol *57*, 499-524.

Cole, J.C., Villa, B.R., and Wilkinson, R.S. (2000). Disruption of actin impedes transmitter release in snake motor terminals. J Physiol *525 Pt 3*, 579-586.

Cote, R.H., and Borisy, G.G. (1981). Head-to-tail polymerization of microtubules in vitro. J Mol Biol *150*, 577-599.

Cumming, R., Burgoyne, R.D., Lytton, N.A., and Gray, E.G. (1983). Immunocytochemical evidence for tubulin in the presynaptic terminal of synaptosomes. Neurosci Lett *37*, 215-220.

Danik, M., Cassoly, E., Manseau, F., Sotty, F., Mouginot, D., and Williams, S. (2005). Frequent coexpression of the vesicular glutamate transporter 1 and 2 genes, as well as coexpression with genes for choline acetyltransferase or glutamic acid decarboxylase in neurons of rat brain. J Neurosci Res *81*, 506-521.

Darcy, K.J., Staras, K., Collinson, L.M., and Goda, Y. (2006). Constitutive sharing of recycling synaptic vesicles between presynaptic boutons. Nat Neurosci *9*, 315-321.

de Lange, R.P., de Roos, A.D., and Borst, J.G. (2003). Two modes of vesicle recycling in the rat calyx of Held. J Neurosci *23*, 10164-10173.

Del Castillo, J., and Katz, B. (1954). Quantal components of the end-plate potential. J Physiol *124*, 560-573.

Delvendahl, I., Vyleta, N.P., von Gersdorff, H., and Hallermann, S. (2016). Fast, Temperature-Sensitive and Clathrin-Independent Endocytosis at Central Synapses. Neuron *90*, 492-498.

Dimitrov, D., Guillaud, L., Eguchi, K., and Takahashi, T. (2018). Culture of Mouse Giant Central Nervous System Synapses and Application for Imaging and Electrophysiological Analyses. Methods Mol Biol *1727*, 201-215.

Dimitrov, D., Takagi, H., Guillaud, L., Saitoh, N., Eguchi, K., and Takahashi, T. (2016). Reconstitution of Giant Mammalian Synapses in Culture for Molecular Functional and Imaging Studies. J Neurosci *36*, 3600-3610.

Dunaevsky, A., and Connor, E.A. (2000). F-actin is concentrated in nonrelease domains at frog neuromuscular junctions. J Neurosci *20*, 6007-6012.

Edwards, F.A., Konnerth, A., Sakmann, B., and Takahashi, T. (1989). A thin slice preparation for patch clamp recordings from neurones of the mammalian central nervous system. Pflugers Arch *414*, 600-612.

Engqvist-Goldstein, A.E., and Drubin, D.G. (2003). Actin assembly and endocytosis: from yeast to mammals. Annu Rev Cell Dev Biol *19*, 287-332.

Feit, H., and Barondes, S.H. (1970). Colchicine-binding activity in particulate fractions of mouse brain. J Neurochem *17*, 1355-1364.

Feit, H., Dutton, G.R., Barondes, S.H., and Shelanski, M.L. (1971). Microtubule protein. Identification in and transport to nerve endings. J Cell Biol *51*, 138-147.

Fukazawa, Y., Saitoh, Y., Ozawa, F., Ohta, Y., Mizuno, K., and Inokuchi, K. (2003). Hippocampal LTP is accompanied by enhanced F-actin content within the dendritic spine that is essential for late LTP maintenance in vivo. Neuron *38*, 447-460.

Gandini, M.A., Henriquez, D.R., Grimaldo, L., Sandoval, A., Altier, C., Zamponi, G.W., Felix, R., and Gonzalez-Billault, C. (2014). $Ca_V2.2$ channel cell surface expression is regulated by the light chain 1 (LC1) of the microtubule-associated protein B (MAP1B) via UBE2L3-mediated ubiquitination and degradation. Pflugers Arch *466*, 2113-2126.

Geiger, J.R., Melcher, T., Koh, D.S., Sakmann, B., Seeburg, P.H., Jonas, P., and Monyer, H. (1995). Relative abundance of subunit mRNAs determines gating and Ca^{2+} permeability of AMPA receptors in principal neurons and interneurons in rat CNS. Neuron *15*, 193-204.

Gotow, T., Miyaguchi, K., and Hashimoto, P.H. (1991). Cytoplasmic architecture of the axon terminal: filamentous strands specifically associated with synaptic vesicles. Neuroscience *40*, 587-598.

Graffe, M., Zenisek, D., and Taraska, J.W. (2015). A marginal band of microtubules transports and organizes mitochondria in retinal bipolar synaptic terminals. J Gen Physiol *146*, 109-117.

Gras, C., Herzog, E., Bellenchi, G.C., Bernard, V., Ravassard, P., Pohl, M., Gasnier, B., Giros, B., and El Mestikawy, S. (2002). A Third Vesicular Glutamate Transporter Expressed by Cholinergic and Serotoninergic Neurons. J Neurosci *22*, 5442-5451.

Gras, C., Vinatier, J., Amilhon, B., Guerci, A., Christov, C., Ravassard, P., Giros, B., and El Mestikawy, S. (2005). Developmentally regulated expression of VGLUT3 during early post-natal life. Neuropharmacology *49*, 901-911.

Gray, E.G. (1975). Presynaptic microtubules and their association with synaptic vesicles. Proc R Soc Lond B Biol Sci *190*, 367-372.

Gray, E.G. (1983). Neurotransmitter release mechanisms and microtubules. Proc R Soc Lond B Biol Sci *218*, 253-258.

Greengard, P., Benfenati, F., and Valtorta, F. (1994). Synapsin I, an actin-binding protein regulating synaptic vesicle traffic in the nerve terminal. Adv Sec Mess Phospho Res *29*, 31-45.

Guillaud, L., Dimitrov, D., and Takahashi, T. (2017). Presynaptic morphology and vesicular composition determine vesicle dynamics in mouse central synapses. eLife *6*.

Hajos, F., Csillag, A., and Kalman, M. (1979). The morphology of microtubules in incubated synaptosomes. Effect of low temperature and vinblastine. Exp Brain Res *35*, 387-393.

Hamann, M., Billups, B., and Forsythe, I.D. (2003). Non-calyceal excitatory inputs mediate low fidelity synaptic transmission in rat auditory brainstem slices. Eur J Neurosci *18*, 2899-2902.

Heuser, J.E., and Reese, T.S. (1973). Evidence for recycling of synaptic vesicle membrane during transmitter release at the frog neuromuscular junction. J Cell Biol *57*, 315-344.

Hilfiker, S., Pieribone, V.A., Czernik, A.J., Kao, H.T., Augustine, G.J., and Greengard, P. (1999). Synapsins as regulators of neurotransmitter release. Philos Trans R Soc Lond B Biol Sci *354*, 269-279.

Hirokawa, N., Sobue, K., Kanda, K., Harada, A., and Yorifuji, H. (1989). The cytoskeletal architecture of the presynaptic terminal and molecular structure of synapsin 1. J Cell Biol *108*, 111-126.

Holderith, N., Lorincz, A., Katona, G., Rozsa, B., Kulik, A., Watanabe, M., and Nusser, Z. (2012). Release probability of hippocampal glutamatergic terminals scales with the size of the active zone. Nat Neurosci *15*, 988-997.

Honda, A., Yamada, M., Saisu, H., Takahashi, H., Mori, K.J., and Abe, T. (2002). Direct, Ca^{2+}-dependent interaction between tubulin and synaptotagmin I: a possible mechanism for attaching synaptic vesicles to microtubules. J Biol Chem *277*, 20234-20242.

Hori, T., and Takahashi, T. (2012). Kinetics of synaptic vesicle refilling with neurotransmitter glutamate. Neuron *76*, 511-517.

Hosoi, N., Sakaba, T., and Neher, E. (2007). Quantitative analysis of calcium-dependent vesicle recruitment and its functional role at the calyx of Held synapse. J Neurosci *27*, 14286-14298.

Hua, Z., Leal-Ortiz, S., Foss, S.M., Waites, C.L., Garner, C.C., Voglmaier, S.M., and Edwards, R.H. (2011). v-SNARE composition distinguishes synaptic vesicle pools. Neuron *71*, 474-487.

Hummel, T., Krukkert, K., Roos, J., Davis, G., and Klambt, C. (2000). Drosophila Futsch/22C10 is a MAP1B-like protein required for dendritic and axonal development. Neuron *26*, 357-370.

Ishikawa, T., Sahara, Y., and Takahashi, T. (2002). A single packet of transmitter does not saturate postsynaptic glutamate receptors. Neuron *34*, 613-621.

Iwasaki, S., Momiyama, A., Uchitel, O.D., and Takahashi, T. (2000). Developmental changes in calcium channel types mediating central synaptic transmission. J Neurosci *20*, 59-65.

Iwasaki, S., and Takahashi, T. (1998). Developmental changes in calcium channel types mediating synaptic transmission in rat auditory brainstem. J Physiol *509 (Pt 2)*, 419-423.

Jonas, E.A., Buchanan, J., and Kaczmarek, L.K. (1999). Prolonged activation of mitochondrial conductances during synaptic transmission. Science *286*, 1347-1350.

Jordan, M.A., Thrower, D., and Wilson, L. (1992). Effects of vinblastine, podophyllotoxin and nocodazole on mitotic spindles. Implications for the role of microtubule dynamics in mitosis. J Cell Sci *102 (Pt 3)*, 401-416.

Jordan, R., Lemke, E.A., and Klingauf, J. (2005). Visualization of synaptic vesicle movement in intact synaptic boutons using fluorescence fluctuation spectroscopy. Biophys J *89*, 2091-2102.

Kadota, T., Kadota, K., and Gray, E.G. (1976). Coated-vesicle shells, particle/chain material, and tubulin in brain synaptosomes. An electron microscope and biochemical study. J Cell Biol *69*, 608-621.

Katz, B., and Miledi, R. (1969). Spontaneous and evoked activity of motor nerve endings in calcium Ringer. J Physiol *203*, 689-706.

Kerr, A.M., Reisinger, E., and Jonas, P. (2008). Differential dependence of phasic transmitter release on synaptotagmin 1 at GABAergic and glutamatergic hippocampal synapses. Proc Natl Acad Sci U S A *105*, 15581-15586.

Kim, C.H., and Lisman, J.E. (1999). A role of actin filament in synaptic transmission and long-term potentiation. J Neurosci *19*, 4314-4324.

Kirsch, J., and Betz, H. (1995). The postsynaptic localization of the glycine receptor-associated protein gephyrin is regulated by the cytoskeleton. J Neurosci *15*, 4148-4156.

Koike-Tani, M., Saitoh, N., and Takahashi, T. (2005). Mechanisms underlying developmental speeding in AMPA-EPSC decay time at the calyx of Held. J Neurosci *25*, 199-207.

Kononenko, N.L., Puchkov, D., Classen, G.A., Walter, A.M., Pechstein, A., Sawade, L., Kaempf, N., Trimbuch, T., Lorenz, D., Rosenmund, C., *et al.* (2014). Clathrin/AP-2 mediate synaptic vesicle reformation from endosome-like vacuoles but are not essential for membrane retrieval at central synapses. Neuron *82*, 981-988.

Krucker, T., Siggins, G.R., and Halpain, S. (2000). Dynamic actin filaments are required for stable long-term potentiation (LTP) in area CA1 of the hippocampus. Proc Natl Acad Sci U S A *97*, 6856-6861.

Kuromi, H., and Kidokoro, Y. (1998). Two distinct pools of synaptic vesicles in single presynaptic boutons in a temperature-sensitive Drosophila mutant, shibire. Neuron *20*, 917-925.

Kuwabara, N., DiCaprio, R.A., and Zook, J.M. (1991). Afferents to the medial nucleus of the trapezoid body and their collateral projections. J Comp Neurol *314*, 684-706.

Lagnado, J.R., Lyons, C., and Wickremasinghe, G. (1971). The subcellular distribution of colchicine-binding protein ('microtubule protein') in rat brain. FEBS Lett *15*, 254-258.

Landis, D.M., Hall, A.K., Weinstein, L.A., and Reese, T.S. (1988). The organization of cytoplasm at the presynaptic active zone of a central nervous system synapse. Neuron *1*, 201-209.

Lee, J.S., Ho, W.K., and Lee, S.H. (2012a). Actin-dependent rapid recruitment of reluctant synaptic vesicles into a fast-releasing vesicle pool. Proc Natl Acad Sci U S A *109*, E765-774.

Lee, S., Jung, K.J., Jung, H.S., and Chang, S. (2012b). Dynamics of multiple trafficking behaviors of individual synaptic vesicles revealed by quantum-dot based presynaptic probe. PloS one *7*, e38045.

Leenders, A.G., Lin, L., Huang, L.D., Gerwin, C., Lu, P.H., and Sheng, Z.H. (2008). The role of MAP1A light chain 2 in synaptic surface retention of $Ca_v2.2$ channels in hippocampal neurons. J Neurosci *28*, 11333-11346.

Lepicard, S., Franco, B., de Bock, F., and Parmentier, M.L. (2014). A presynaptic role of microtubule-associated protein 1/Futsch in Drosophila: regulation of active zone number and neurotransmitter release. J Neurosci *34*, 6759-6771.

Li, Z., and Murthy, V.N. (2001). Visualizing postendocytic traffic of synaptic vesicles at hippocampal synapses. Neuron *31*, 593-605.

Lin, B., Kramar, E.A., Bi, X., Brucher, F.A., Gall, C.M., and Lynch, G. (2005). Theta stimulation polymerizes actin in dendritic spines of hippocampus. J Neurosci *25*, 2062-2069.

Llinas, R., Gruner, J.A., Sugimori, M., McGuinness, T.L., and Greengard, P. (1991). Regulation by synapsin I and Ca^{2+}-calmodulin-dependent protein kinase II of the transmitter release in squid giant synapse. J Physiol *436*, 257-282.

Lukinavicius, G., Reymond, L., D'Este, E., Masharina, A., Gottfert, F., Ta, H., Guther, A., Fournier, M., Rizzo, S., Waldmann, H., *et al.* (2014). Fluorogenic probes for live-cell imaging of the cytoskeleton. Nat Methods *11*, 731-733.

Luo, F., and Sudhof, T.C. (2017). Synaptotagmin-7-Mediated Asynchronous Release Boosts High-Fidelity Synchronous Transmission at a Central Synapse. Neuron *94*, 826-839.e823.

Matus, A., Bernhardt, R., and Hugh-Jones, T. (1981). High molecular weight microtubule-associated proteins are preferentially associated with dendritic microtubules in brain. Proc Natl Acad Sci U S A *78*, 3010-3014.

Matus, A.I., Walters, B.B., and Mughal, S. (1975). Immunohistochemical demonstration of tubulin associated with microtubules and synaptic junctions in mammalian brain. J Neurocytol *4*, 733-744.

Maycox, P.R., Deckwerth, T., Hell, J.W., and Jahn, R. (1988a). Glutamate uptake by brain synaptic vesicles. Energy dependence of transport and functional reconstitution in proteoliposomes. J Biol Chem *263*, 15423-15428.

Maycox, P.R., Deckwerth, T., Hell, J.W., and Jahn, R. (1988b). Glutamate uptake by brain synaptic vesicles. Energy dependence of transport and functional reconstitution in proteoliposomes. J Biol Chem *263*, 15423-15428.

McMahon, H.T., and Boucrot, E. (2011). Molecular mechanism and physiological functions of clathrin-mediated endocytosis. Nat Rev Mol Cell Biol *12*, 517-533.

Melia, T.J., Jr. (2007). Putting the clamps on membrane fusion: how complexin sets the stage for calcium-mediated exocytosis. FEBS Lett *581*, 2131-2139.

Meng, Y., Zhang, Y., Tregoubov, V., Janus, C., Cruz, L., Jackson, M., Lu, W.Y., MacDonald, J.F., Wang, J.Y., Falls, D.L., *et al.* (2002). Abnormal spine morphology and enhanced LTP in LIMK-1 knockout mice. Neuron *35*, 121-133.

Miki, T., Hirai, H., and Takahashi, T. (2013). Activity-dependent neurotrophin signaling underlies developmental switch of Ca^{2+} channel subtypes mediating neurotransmitter release. J Neurosci *33*, 18755-18763.

Mitchison, T., and Kirschner, M. (1984). Dynamic instability of microtubule growth. Nature *312*, 237-242.

Mitchison, T.J. (1993). Localization of an exchangeable GTP binding site at the plus end of microtubules. Science *261*, 1044-1047.

Moechars, D., Weston, M.C., Leo, S., Callaerts-Vegh, Z., Goris, I., Daneels, G., Buist, A., Cik, M., van der Spek, P., Kass, S., *et al.* (2006). Vesicular glutamate transporter VGLUT2 expression levels control quantal size and neuropathic pain. J Neurosci *26*, 12055-12066.

Morales, M., Colicos, M.A., and Goda, Y. (2000). Actin-dependent regulation of neurotransmitter release at central synapses. Neuron *27*, 539-550.

Nakamura, T., Yamashita, T., Saitoh, N., and Takahashi, T. (2008). Developmental changes in calcium/calmodulin-dependent inactivation of calcium currents at the rat calyx of Held. J Physiol *586*, 2253-2261.

Nakamura, Y., Harada, H., Kamasawa, N., Matsui, K., Rothman, J.S., Shigemoto, R., Silver, R.A., DiGregorio, D.A., and Takahashi, T. (2015). Nanoscale distribution of presynaptic Ca^{2+}-channels and its impact on vesicular release during development. Neuron *85*, 145-158.

Nakayama, K., and Silverman, G.H. (1986). Serial and parallel processing of visual feature conjunctions. Nature *320*, 264-265.

Neher, E., and Sakaba, T. (2001). Estimating transmitter release rates from postsynaptic current fluctuations. J Neurosci *21*, 9638-9654.

Okamoto, K., Nagai, T., Miyawaki, A., and Hayashi, Y. (2004). Rapid and persistent modulation of actin dynamics regulates postsynaptic reorganization underlying bidirectional plasticity. Nat Neurosci *7*, 1104-1112.

Pang, Z.P., Shin, O.H., Meyer, A.C., Rosenmund, C., and Sudhof, T.C. (2006). A gain-of-function mutation in synaptotagmin-1 reveals a critical role of Ca^{2+}-dependent soluble N-ethylmaleimide-sensitive factor attachment protein receptor complex binding in synaptic exocytosis. J Neurosci *26*, 12556-12565.

Paxinos, G. and Watson, C. (1982). The rat brain in stereotaxic coordinates. Academic Press.

Perkins, G.A., Tjong, J., Brown, J.M., Poquiz, P.H., Scott, R.T., Kolson, D.R., Ellisman, M.H., and Spirou, G.A. (2010). The micro-architecture of mitochondria at active zones: electron tomography reveals novel anchoring scaffolds and cristae structured for high-rate metabolism. J Neurosci *30*, 1015-1026.

Qiu, X., Zhu, Q., and Sun, J. (2015). Quantitative analysis of vesicle recycling at the calyx of Held synapse. Proc Natl Acad Sci U S A *112*, 4779-4784.

Rea, R., Li, J., Dharia, A., Levitan, E.S., Sterling, P., and Kramer, R.H. (2004). Streamlined synaptic vesicle cycle in cone photoreceptor terminals. Neuron *41*, 755-766.

Richards, D.A., Rizzoli, S.O., and Betz, W.J. (2004). Effects of wortmannin and latrunculin A on slow endocytosis at the frog neuromuscular junction. J Physiol *557*, 77-91.

Rizo, J., and Rosenmund, C. (2008). Synaptic vesicle fusion. Nat Struct Mol Biol *15*, 665-674.

Rizzoli, S.O., and Betz, W.J. (2005). Synaptic vesicle pools. Nat Rev Neurosci *6*, 57-69.

Roos, J., Hummel, T., Ng, N., Klambt, C., and Davis, G.W. (2000). Drosophila Futsch regulates synaptic microtubule organization and is necessary for synaptic growth. Neuron *26*, 371-382.

Rothman, J.S., Kocsis, L., Herzog, E., Nusser, Z., and Silver, R.A. (2016). Physical determinants of vesicle mobility and supply at a central synapse. eLife *5*.

Ryan, T.A. (1999). Inhibitors of myosin light chain kinase block synaptic vesicle pool mobilization during action potential firing. J Neurosci *19*, 1317-1323.

Sahara, Y., and Takahashi, T. (2001). Quantal components of the excitatory postsynaptic currents at a rat central auditory synapse. J Physiol *536*, 189-197.

Saitoh, N., Hori, T., and Takahashi, T. (2001). Activation of the epsilon isoform of protein kinase C in the mammalian nerve terminal. PNAS *98*, 14017-14021.

Sakaba, T., and Neher, E. (2001a). Calmodulin mediates rapid recruitment of fast-releasing synaptic vesicles at a calyx-type synapse. Neuron *32*, 1119-1131.

Sakaba, T., and Neher, E. (2001b). Quantitative relationship between transmitter release and calcium current at the calyx of held synapse. J Neurosci *21*, 462-476.

Sakaba, T., and Neher, E. (2003). Involvement of actin polymerization in vesicle recruitment at the calyx of Held synapse. J Neurosci *23*, 837-846.

Sankaranarayanan, S., Atluri, P.P., and Ryan, T.A. (2003). Actin has a molecular scaffolding, not propulsive, role in presynaptic function. Nat Neurosci *6*, 127-135.

Sara, Y., Virmani, T., Deak, F., Liu, X., and Kavalali, E.T. (2005). An isolated pool of vesicles recycles at rest and drives spontaneous neurotransmission. Neuron *45*, 563-573.

Satzler, K., Sohl, L.F., Bollmann, J.H., Borst, J.G., Frotscher, M., Sakmann, B., and Lubke, J.H. (2002). Three-dimensional reconstruction of a calyx of Held and its postsynaptic principal neuron in the medial nucleus of the trapezoid body. J Neurosci *22*, 10567-10579.

Schmitt, F.O. (1968). Fibrous proteins--neuronal organelles. Proc Natl Acad Sci U S A *60*, 1092-1101.

Schnapp, B.J., and Reese, T.S. (1982). Cytoplasmic structure in rapid-frozen axons. J Cell Biol *94*, 667-669.

Schneggenburger, R., Meyer, A.C., and Neher, E. (1999). Released fraction and total size of a pool of immediately available transmitter quanta at a calyx synapse. Neuron *23*, 399-409.

Schoch, S., Castillo, P.E., Jo, T., Mukherjee, K., Geppert, M., Wang, Y., Schmitz, F., Malenka, R.C., and Sudhof, T.C. (2002). RIM1alpha forms a protein scaffold for regulating neurotransmitter release at the active zone. Nature *415*, 321-326.

Seal, R.P., and Edwards, R.H. (2006). The diverse roles of vesicular glutamate transporter 3. Handbook of experimental pharmacology, 137-150.

Sherrington, C.S. (1906). Observations on the scratch-reflex in the spinal dog. J Physiol *34*, 1-50.

Shupliakov, O., Bloom, O., Gustafsson, J.S., Kjaerulff, O., Low, P., Tomilin, N., Pieribone, V.A., Greengard, P., and Brodin, L. (2002). Impaired recycling of synaptic vesicles after acute perturbation of the presynaptic actin cytoskeleton. Proc Natl Acad Sci U S A *99*, 14476-14481.

Smith, D.S., Jarlfors, U., and Beranek, R. (1970). The organization of synaptic axcplasm in the lamprey (petromyzon marinus) central nervous system. J Cell Biol *46*, 199-219.

Sollner, T., Whiteheart, S.W., Brunner, M., Erdjument-Bromage, H., Geromanos, S., Tempst, P., and Rothman, J.E. (1993). SNAP receptors implicated in vesicle targeting and fusion. Nature *362*, 318-324.

Sudhof, T.C., and Rothman, J.E. (2009). Membrane fusion: grappling with SNARE and SM proteins. Science *323*, 474-477.

Sun, J.Y., Wu, X.S., and Wu, L.G. (2002). Single and multiple vesicle fusion induce different rates of endocytosis at a central synapse. Nature *417*, 555-559.

Takahashi, T. (1978). Intracellular recording from visually identified motoneurons in rat spinal cord slices. Proc R Soc Lond B Biol Sci *202*, 417-421.

Tang, Y., and Zucker, R.S. (1997). Mitochondrial involvement in post-tetanic potentiation of synaptic transmission. Neuron *18*, 483-491.

Taschenberger, H., Leao, R.M., Rowland, K.C., Spirou, G.A., and von Gersdorff, H. (2002). Optimizing synaptic architecture and efficiency for high-frequency transmission. Neuron *36*, 1127-1143.

Wadel, K., Neher, E., and Sakaba, T. (2007). The coupling between synaptic vesicles and Ca^{2+} channels determines fast neurotransmitter release. Neuron *53*, 563-575.

Watanabe, S., Rost, B.R., Camacho-Perez, M., Davis, M.W., Sohl-Kielczynski, B., Rosenmund, C., and Jorgensen, E.M. (2013). Ultrafast endocytosis at mouse hippocampal synapses. Nature *504*, 242-247.

Wilhelm, B.G., Mandad, S., Truckenbrodt, S., Krohnert, K., Schafer, C., Rammner, B., Koo, S.J., Classen, G.A., Krauss, M., Haucke, V., *et al.* (2014). Composition of isolated synaptic boutons reveals the amounts of vesicle trafficking proteins. Science *344*, 1023-1028.

Wilson, N.R., Kang, J., Hueske, E.V., Leung, T., Varoqui, H., Murnick, J.G., Erickson, J.D., and Liu, G. (2005). Presynaptic Regulation of Quantal Size by the Vesicular Glutamate Transporter VGLUT1. The Journal of Neuroscience *25*, 6221-6234.

Wolosker, H., de Souza, D.O., and de Meis, L. (1996). Regulation of Glutamate Transport into Synaptic Vesicles by Chloride and Proton Gradient. J Biol Chem *271*, 11726-11731.

Wu, L.G., and Borst, J.G. (1999). The reduced release probability of releasable vesicles during recovery from short-term synaptic depression. Neuron *23*, 821-832.

Wu, L.G., Borst, J.G., and Sakmann, B. (1998). R-type Ca^{2+} currents evoke transmitter release at a rat central synapse. Proc Natl Acad Sci U S A *95*, 4720-4725.

Wu, L.G., Westenbroek, R.E., Borst, J.G., Catterall, W.A., and Sakmann, B. (1999). Calcium channel types with distinct presynaptic localization couple differentially to transmitter release in single calyx-type synapses. J Neurosci *19*, 726-736.

Wu, X.S., Lee, S.H., Sheng, J., Zhang, Z., Zhao, W.D., Wang, D., Jin, Y., Charnay, P., Ervasti, J.M., and Wu, L.G. (2016). Actin Is Crucial for All Kinetically Distinguishable Forms of Endocytosis at Synapses. Neuron *92*, 1020-1035.

Xu, J., Mashimo, T., and Sudhof, T.C. (2007). Synaptotagmin-1, -2, and -9: Ca^{2+} sensors for fast release that specify distinct presynaptic properties in subsets of neurons. Neuron *54*, 567-581.

Xu, J., and Wu, L.G. (2005). The decrease in the presynaptic calcium current is a major cause of short-term depression at a calyx-type synapse. Neuron *46*, 633-645.

Yamashita, M., Kawaguchi, S., Hori, T., and Takahashi, T. (2018). Vesicular GABA uptake can be Rate-Limiting for Recovery of IPSCs from Synaptic Depression. Cell Reports, *In press*.

Yamashita, T., Eguchi, K., Saitoh, N., von Gersdorff, H., and Takahashi, T. (2010). Developmental shift to a mechanism of synaptic vesicle endocytosis requiring nanodomain Ca^{2+}. Nat Neurosci *13*, 838-844.

Yamashita, T., Hige, T., and Takahashi, T. (2005). Vesicle endocytosis requires dynamin-dependent GTP hydrolysis at a fast CNS synapse. Science *307*, 124-127.

Zilly, F.E., Sorensen, J.B., Jahn, R., and Lang, T. (2006). Munc18-bound syntaxin readily forms SNARE complexes with synaptobrevin in native plasma membranes. PLoS Biol *4*, e330.